Enhancing medication delivery of eluting stents: a computationally aided parametric approach

Jack Poulton

Department of Mechanical Engineering

McGill University, Montreal

March 2024

A thesis submitted to McGill University in partial fulfillment of the requirements of the degree of Master of Science in Engineering

Contents

List of Acronyms, Nomenclature, and Key Terms

Term	Definition
Restenosis	Reduction in lumen diameter following angioplasty or percutaneous coronary intervention
Percutaneous Coronary Intervention	A non-surgical procedure used to treat atherosclerosis using angioplasty and stent implantation
ISR	In-Stent Restenosis
PMSC-NV	PREY mesenchymal stem cell-derived nanovesicles
Monocyte	White blood cell
LDL	Low-Density Lipoprotein
HDL	High-Density Lipoprotein
Macrophage	A type of white blood cell that engulfs and ingests targeted agents within the body
T Lymphocyte	A member of the body's immune response that destroys infected host cells, produces cytokines, and activates other immune cells
Cytokines	Proteins that control the growth and activity of other immune system cells and blood cells
ROS	Reactive Oxygen Species
Hematocrit	Percentage of blood, by volume that is composed of red blood cells
UDS	User Defined Scalar
RMSE	Root Mean Squared Error

List of Figures

List of Tables

Abstract

The advancements made in stent technology have drastically improved the efficacy of percutaneous coronary interventions. The previously high rates of restenosis associated with bare-metal stents have nearly vanished. This is largely due to the creation of drug-eluting stents. However, high rates of late stent thrombosis continue to put patients' lives at risk. The distribution of the eluted medicine once diffused into the artery, has been identified as a controllable factor that can influence patient outcomes. In this study, a computational fluid dynamics analysis of a stented arterial section was performed to determine the influence of stent geometry and eluting particle diffusion coefficient on particle distribution in an artery. The results show trends in stent geometry that have both spatial and temporal dependence. Shortly after implantation, arterial regions nearest to the lumen will experience the highest particle concentration homogeneity with a large stent surface. As the depth from the lumen grows, the relationship flips, and smaller surfaces provide improved particle distribution variance. The trends in uniformity are affected by time, as they begin to favor smaller stent surfaces when compared to their younger counterparts. The diffusion coefficient was found to impact all regions and times similarly. The cases with the largest diffusion coefficient consistently outperformed those with smaller values. These results indicate that the size of the artery, the intended window of action of the eluted medication, and the properties of the eluted medication are all factors that must be considered when designing an eluting stent.

Résumé

Les progrès réalisés dans la technologie des stents ont considérablement amélioré l'efficacité des interventions coronariennes percutanées. Les taux de resténose, autrefois élevés, associés aux stents en métal nu ont pratiquement disparu. Cela est dû en grande partie à la création des stents à élution médicamenteuse. Cependant, les taux élevés de thrombose tardive du stent continuent de mettre la vie des patients en danger. La distribution du médicament élué, une fois diffusé dans l'artère, a été identifiée comme un facteur contrôlable pouvant influencer les résultats pour les patients. Dans cette étude, une analyse numérique de la dynamique des fluides d'une section artérielle stentée a été réalisée pour déterminer l'influence de la géométrie du stent et du coefficient de diffusion des particules d'élution sur la distribution des particules dans une artère. Les résultats montrent des tendances dans la géométrie de l'endoprothèse qui ont une dépendance à la fois spatiale et temporelle. Peu après l'implantation, les régions artérielles les plus proches de la lumière présentent l'homogénéité de concentration de particules la plus élevée avec une grande surface de stent. Au fur et à mesure que l'on s'éloigne de la lumière, la relation s'inverse et des surfaces plus petites améliorent la variance de la distribution des particules. Les tendances en matière d'uniformité sont influencées par le temps, car elles commencent à favoriser les petites surfaces de stent par rapport à leurs homologues plus jeunes. Le coefficient de diffusion a un impact similaire sur toutes les régions et tous les temps. Les cas présentant le coefficient de diffusion le plus élevé sont systématiquement plus performants que ceux présentant des valeurs plus faibles. Ces résultats indiquent que la taille de l'artère, la fenêtre d'action prévue du médicament élué et les

propriétés du médicament élué sont autant de facteurs qui doivent être pris en compte lors de la conception d'un stent à élution.

Acknowledgments

I am deeply grateful to my supervisor Dr. Rosaire Mongrain for providing the unwavering support and guidance that I needed over the past two years. Special thanks go to Dr. Hristo Valtchanov, whose patience and wisdom were crucial in making my research possible. I would also like to thank Dr. Jeong-Kee Yoon, Dotter Inc., and Seido Photonics for providing their resources and expertise. To Gregory Doyle, thank you. The mechanical engineering department at McGill runs because of you.

I would like to acknowledge both my parents for all your love, support, and sacrifice. Everything I am and everything I will ever accomplish I owe to you. To my brother, Matthew, for inspiring me to always be a better person. To my friends, thank you for your support and welcome distraction. I would like to especially thank two of my teachers, Vanessa Tellier and Bryan McAlpine. I would never have been able to make it to the positions that I have without your influence. The work ethic and love for learning that you instilled within me have been invaluable in helping me get to where I am today. I would not have been able to reach this point alone. The help I have gotten along the way has been essential. To the community of people who have allowed me to develop the skills I needed or to those who helped keep me sane throughout, I am forever grateful. I offer you my humble appreciation, thank you.

Sincerely,

Jack Poulton

1.0 Introduction

The World Heart Foundation has reported that 20.5 million deaths in 2021 were attributed to cardiovascular diseases, making it the leading cause of death worldwide [1]. Heart failure, a condition which is commonly caused by cardiovascular diseases, is a life-threatening affliction that affects more than 26 million people [2]. The 10-year survival rate of untreated heart failure is 34.9%, a rate more lethal than both breast cancer and prostate cancer [2] [3]. Not all forms of cardiovascular diseases are immediately fatal. The milder cases can be treated with daily medication or simple lifestyle changes. Unfortunately, these solutions are unsuitable for some patients, and much more drastic methods are required. One such treatment method is percutaneous coronary intervention. In the United States alone, more than 600,000 coronary stents are implanted every year [4].

In January of 1964, an 83-year-old woman was admitted to the Oregon Health Sciences University Hospital with a nonhealing foot ulcer and gangrenous toes. The cause was poor circulation, which had been deemed beyond repair, and amputation was prescribed as the only possible solution. The patient outright refused the treatment. Instead, Charles Dotter, the hospital's radiologist, pioneered a new technique as a last-ditch effort to save the patient's foot. He inserted a small wire into the buildup of plaque that was occluding the patient's superficial femoral artery. He then used progressively larger catheters to clear the blockage. Within weeks the woman's ulcer had healed and the pain had completely resolved [5]. This procedure was known as "Dottering" and became the standard for treating obstructed arteries. As its popularity grew, it was modified, and in 1977 the first balloon angioplasty took place [5].

However, as the number of angioplasty procedures grew, the patient outcome data showed a worrying trend. Patients who had undergone angioplasty were suffering from alarmingly high restenosis rates, with some reports of up to 48% [5]. At the time, cardiologists were focused on procedural dissection-related acute vessel closure and late restenosis caused by elastic recoil of vascular tissue [6]. A solution came in 1986 when the first stent was implanted. In addition to angioplasty, a small, meshed tube was inserted into the artery [7]. The rigid stent structure was successful in mitigating the restenosis caused by the elastic recoil of the artery. Overgrowth of vascular tissue into the lumen, a side effect of stenting, led to the development of drug-eluting stents (DES). In this treatment method, the stent's metallic scaffold is coated with a drug-eluting layer. When diffused into the artery, the drugs prevent the proliferation of smooth muscle and endothelial cells. This technique, while successfully reducing in-stent restenosis (ISR) rates, can cause late-stent thrombosis. The same drugs that prevent the overgrowth of the arterial tissue that causes ISR, also prevent proper vascular healing. Incomplete healing leaves the artery susceptible to thrombus formation. A proposed solution is to replace the drug in the coating with mesenchymal stem cell-derived nanovesicles that contain the peptide GSPREYTSYMPH (PMSC-NVs). These PMSC-NVs provide the needed anti-inflammatory effects while also promoting endothelial recovery, which prevents the formation of late-stent thrombosis [8].

In this study, a scaffold design, provided by Dotter Inc. (Seoul, Republic of Korea), and vasculature were modeled and analysed using ANSYS Fluent. A parametric analysis was conducted with particle uniformity in the artery wall as the objective. The diffusion of the particles was modeled as a flux off the surface of the scaffold into the artery. The PMSC-NVs were the eluting particles used in the simulation. The aim was to explore the diffusion process

of these PMSC-NVs with different diffusion properties and scaffold geometries to assess the influence these factors have on the uniformity of the particle concentration distribution in the artery wall.

2.0 Literature Review

2.1 Artery Anatomy

Arteries are a key member of the cardiovascular system, managing the transportation of oxygen, nutrients, and hormones throughout the body via the blood [9]. Along with the heart, these vessels help form the pressure wave that drives blood flow, doing so by contracting or dilating the lumen. Through contraction and dilation, arteries play a role in the body's response to external temperature, pressure, and substances. Artery physiology is strongly influenced by the three distinct layers that comprise them. These layers, which have varying sizes and compositions, are displayed in Figure 1 below.

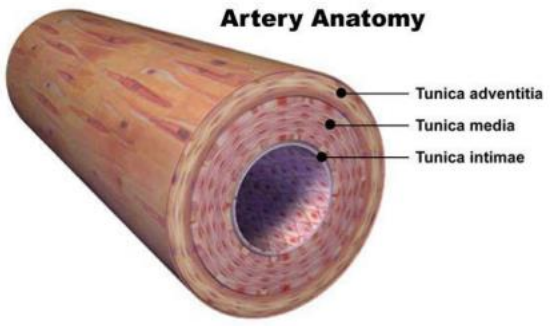

Figure 1: Artery wall anatomy and the three layers that compose the wall, adapted from [10].

2.1.1 Tunica Intimae

The innermost layer of the artery is the tunica intimae. It is one layer of endothelial cells thick and is composed of endothelial cells and their basal lamina, type IV collagen, fibronectin,

and laminin [11]. The elements that comprise the tunica intimae create highly elastic properties. The hollow interior of the artery, called the lumen, is formed by the tunica intimae. As blood flows through the lumen, the endothelial cells of the tunica intimae act as an interface between the components in the blood and the rest of the artery wall.

2.1.2 Tunica Media

The start of the tunica media is marked by the presence of a thin elastin-rich ring known as the internal elastic lamina. The tunica media is the thickest of the three layers and is composed of smooth muscle cells, elastin, type I, III, and V collagen, and proteoglycans [11]. The smooth muscle cells of the media are oriented circumferentially. This alignment allows smooth muscle cell contraction to form the pressure wave that drives blood flow. Collagen is aligned in a similar direction to the smooth muscle cells but also forms a slight helical pattern. Due to the smooth muscle cells that are present, the media is the most rigid of the three sections of the artery. The collagen acts to provide the structural support of the media. The thickness and structure of the media differ between arteries. As the driver of arterial constriction and dilation, some arteries, which experience higher pressures, have thicker media and are composed of a larger percentage of smooth muscle cells [11]. The tunica media ends with the outer elastic lamina, separating it from the tunica adventitia.

2.1.3 Tunica Adventitia

The tunica adventitia is the outermost layer of the arterial wall and is composed of loose connective tissue, type I collagen, nerves, fibroblasts, and elastin. The tunica adventitia serves two functions; receiving contractile signals from the vascular nerves and helping to tether arteries to the surrounding connective tissue [9].

2.2 Atherosclerosis

Atherosclerosis is the occlusion of an artery. It commonly occurs as a result of sudden rupture of the endothelial wall lining the tunica intimae, leading to thrombosis [12]. The clot formed due to thrombosis causes the near-complete blockage of the artery. The causes of this process are complex and still not entirely understood. Low-density lipoproteins (LDLs) have been recognized for quite some time as a key contributor to the onset of atherosclerosis. It was also believed that high-density lipoproteins (HDLs) acted to mitigate the risks of LDLs [13]. However, recent studies contradict this hypothesis. Patients who have suffered from atherosclerosis are now being found with low levels of LDLs and abnormally high levels of HDLs [13]. New work has also found that the inflammatory pathway from the inflammasome through interleukin IL-1 to IL-6 may also be a cause of atherosclerosis [14]. Despite improvements in treatment modalities, the mortality rates of cardiovascular diseases are on the rise, suggesting a lack of a full understanding of the underlying mechanisms that cause atherosclerosis as well as proper mitigation methods [15].

2.2.1 Atherosclerotic Plaque Formation

Endothelial cells form a barrier for molecular transport between the blood and tissues. These cells form a matrix, allowing certain molecules, such as LDLs, to pass through. When the concentration of LDLs in the blood is high, some LDLs become trapped in the endothelial cell matrix [12]. While stuck in the matrix, the trapped LDLs begin to undergo oxidation and glycation. This process activates the body's immune system. The endothelial cells that line the arterial wall have adhesion molecules on their blood-facing sides that attach to monocytes circulating in the bloodstream. The smooth muscle cells and endothelial cells of the tunica

intimae also begin to release chemokines, which further attract monocytes to the area. Once reaching the tunica intimae, the monocytes that have been drawn to the location of high LDL concentration develop into macrophages. Macrophages engulf the LDLs and activate T lymphocytes, which secrete proinflammatory cytokines and chemokines, resulting in a feedback loop that exacerbates the process by drawing in more monocytes [16]. The macrophages ingest the LDLs, eventually becoming so filled with fatty droplets that they appear foamy, and thus, are known as foam cells. The foam cells and T lymphocytes become an early form of atherosclerotic plaque. To protect the tunica intimae from rupture, smooth muscle cells migrate from the tunica media to the tunica intimae. There, smooth muscle cells multiply and form a tough matrix called the cap. The cap is composed of tough extracellular matrix materials such as collagen and elastin. The cap increases the overall size of the plaque but is necessary for protecting the bloodstream from the contents of the plaque. In most cases, the plaque will grow in a direction that is radially outward, preserving blood flow [12]. Consequently, it is possible for there to be no outward effects despite plaque growth in a patient's arteries and can exist in this state for decades [12]. When the growth of the plaque does intrude into the lumen, blood flow may be restricted, causing a condition known as stenosis. Only 15% of heart attacks are caused by excessive stenosis. The remaining 85% occurs when the fibrous cap containing the plaque breaks open, resulting in a blood clot forming over the rupture. This occurs due to a weakening of the plaque by inflammatory substances. The mitochondria of the cells in the plaque tend to dysfunction, resulting in a reduction of overall ATP production, impairment of mitochondrial regulatory roles, and the release of reactive oxygen species (ROS). The ROS create oxidative stress, resulting in chronic inflammation. Additionally, foam cell death, which causes the release

of the previously ingested lipids, acts to increase the inflammatory response. This causes the weakening of the cap. The inflammatory substances break down the extracellular matrix molecules that comprise the cap and damage the smooth muscle cells. Weakening of the cap may lead to plaque rupture. The foam cells of the plaque display tissue factor, which promotes clotting. When the plaque ruptures, the tissue factor interacts with elements of the blood causing a thrombus to form, preventing the contents of the plaque from spilling out into the bloodstream [12]. If the thrombus grows large enough, it will severely reduce blood flow through the artery, increasing the load on the heart and, over time, causing heart failure.

2.3 Angioplasty

The risks of atherosclerosis are severe and leaving it untreated puts a patient's life in serious jeopardy. There is a clear need for swift and effective treatment to mitigate the dangers. The nonsurgical measures that were used as a treatment method before the use of angioplasty acted to allow the patient to live with the disease but were unsuccessful in fully treating the condition [17]. There are multiple types of angioplasties, but the most common is balloon angioplasty. This technique was developed in 1977, 13 years after Dotter pioneered Dottering [18]. A balloon catheter is inserted into the patient's artery where it is then expanded at the location of atherosclerotic plaque. The goal is to increase the luminal cross-sectional area, which is achieved via three mechanisms: plaque fracture, plaque compression, and stretching of the arterial wall [18]. All three mechanisms play a part, but plaque fracture is the most significant. The expansion of the balloon causes plaque fracture due to the inelastic components of the atheroma [19]. Angioplasty not only reduces the risk of myocardial

infarction, which only occurs in 5% of angioplasty cases but also alleviates common symptoms of atherosclerosis, such as angina, by reducing the flow constriction [20].

Several adverse consequences can result from balloon angioplasty. For optimal results, a balloon that inflates to a diameter that is between 90% to 130% of the unaffected arterial segment is required [21]. Although not normally an issue for the arterial wall, because of the atherosclerotic plaque growth, the diameter of the affected artery will be greatly reduced. An occlusion resulting in less than a reduction of 40% of normal diameter is considered only a mild blockage. As a result, the section of the artery that undergoes angioplasty experiences large strains during the procedure. Within the first hour, complete endothelial denudation is very commonly observed. This is met with a high amount of platelet deposition, which stays high for the first four days following the procedure [22]. Necrosis of smooth muscle cells of the tunica media occurs within the first twenty-four hours. During the healing process, inflammation, recoil, and a buildup of scar tissue can cause the treated artery to experience restenosis. Rates of restenosis from balloon angioplasty are high, affecting nearly one in two patients [5]. Despite the elevated use and research attention received by angioplasty after its first use in 1977, the rates of restenosis remained largely unchanged for the first decade after its creation [19]. Angioplasty on its own is unable to consistently treat atherosclerosis without inducing restenosis, which can lead to death, reinfarctions, and strokes [23].

2.4 Bare Metal Stents

The success of angioplasty in treating atherosclerosis meant that it could not be abandoned completely, but the high rates of restenosis were troubling. Rather than discarding angioplasty as a treatment technique, the medical community sought a method that could be used in conjunction with that procedure. Something that would not interfere with the role that angioplasty needed to play in clearing atherosclerotic blockages, but that would prevent the secondary narrowing that was common post-angioplasty. One such method that was developed is the use of a meshed tube to oppose the recoil of elastic vascular stenoses [24]. The procedure, known as stenting, was first attempted in humans in 1986. A self-expanding stainless-steel mesh was used. The mesh was constrained into a delivery catheter, positioned at the proper location, and then released. The mesh expanded outwards, holding the lumen open [25]. When compared to angioplasty alone, stenting was found to provide significantly superior results. One study found that there is as much as a 10% reduction in risk of restenosis when using balloon angioplasty and stenting versus balloon angioplasty alone [26]. Stenting also creates a larger luminal opening. The expansion of the stent provides additional forces to the vascular wall, helping to further open the lumen. The average atherosclerotic stenosis of patients who require procedural intervention is 83%. Angioplasty typically reduces this amount to 42%. The application of a stent has been found to cause a net stenosis of -3% [27]. Overall rates of procedural success are much higher with the addition of stenting. A study comparing angioplasty alone and stenting in a total of 452 patients found that 95% of stenting procedures were successful, with only an 84% success rate in the angioplasty group [28]. The long-term results also favor stenting. After three years, patients who received angioplasty and no stenting

required revascularization of the lesion 7.7% of the time. Stented patients only required this additional procedure 2.1% of the time [29].

2.4.1 Bare Metal Stent Design

The first stent design, created in 1986, called the WALLSTENT, was self-expanding. Due to the limitations of its delivery system, the clinical utility of the WALLSTENT was limited and it was removed from the market not long after its creation. The first stent to achieve the approval of the Food and Drug Administration was balloon-expanding [30]. A balloon-expandable stent is mounted around a balloon catheter, and when the balloon is expanded, the stent material is plastically strained. When the balloon deflates, the stent stays rigidly open. Balloon-expandable stents remain the most common form of stent application at the time of writing. Post-implantation, balloon-expandable stents have significantly larger radial expansion forces than self-expanding stents. This in turn causes a larger mean diameter and mean volume of the lumen in the stented region [31]. The early designs of balloon-expandable stents had higher rates of ISR than self-expanding stents and incidences of major adverse cardiac events were similar between the two stent expansion methods. However, the lower degree of precision of the application of self-expandable stents resulted in a much lower frequency of usage [32] [33] [34]. The optimal stent needs radial strength but also requires longitudinal flexibility to navigate through vessels before reaching the deployment site [24]. Early stent designs focused on radial strength. They had high metallic density, were bulky, and were challenging to use. This resulted in high incidences of sub-acute stent thrombosis as well as failure in deployment and embolization [30]. The current material of choice for bare metal stents is a cobalt-chromium

alloy. This material allows for high radial strength and corrosion resistance with much thinner struts than the early stent designs.

2.4.2 Bare Metal Stent In-Stent Restenosis

The issue of restenosis, though reduced when compared to angioplasty, still prevails when stenting. After angioplasty, restenosis occurs due to elastic recoil and negative vascular remodeling [35]. Post-stenting, however, restenosis occurs due to a different reason. The application of a stent causes an injury to the endothelium that lines the vascular wall. The endothelial cells of the tunica media are crushed, leading to denudation. This injury initiates the formation of a thin layer of thrombus that covers the vascular and stent surfaces. The damage also initiates an inflammatory response. Monocytes are recruited to the damaged region, the number of which is directly correlated to the neointimal area of the injured endothelium [36]. Endothelial cells proliferate and migrate to the injured surfaces. Smooth muscle cells also migrate to the location of the injured tunica intimae from the tunica media, changing phenotype from contractile to synthetic once reaching the intimae. Alongside the migration of smooth muscle cells and endothelial cells is the creation of a new extracellular matrix in the damaged regions. The matrix structure changes during the healing process, but when completed, is composed of sturdy collagen I and collagen III [36]. Restenosis linked to stenting is the result of over-proliferation of smooth muscle cells and extra-cellular matrix formation, known as neointimal hyperplasia. Autopsies have revealed that restenotic tissue from stenting was composed of larger areas of smooth muscle cells and endothelial cells and lower areas of macrophages, collagen, and tissue factor when compared to balloon angioplasty [35]. Stenting is effective at preventing restenosis as a result of elastic recoil but causes the injury that results

in restenosis due to neointimal hyperplasia. By 1999, over ten years after the implementation of stenting, rates of ISR were still being reported to be as high as 30%, indicating a lack of success in stenting's attempt to prevent restenosis [30].

2.5 Drug-Eluting Stents

The shortcomings of the original stents were clear. Preventing restenosis due to elastic recoil of vascular tissue was achievable with the initial designs but the prevention of hyperplasia of smooth muscle cells and endothelial cells into the lumen was not attainable. One solution that was found was to apply a drug-carrying coating to the outer surface of the stent scaffold. The two most common drugs that are used are sirolimus and paclitaxel. When the stent is expanded in the artery, these drugs diffuse into the tissue and deactivate pathways that cause smooth muscle and endothelial cell proliferation and migration [37]. The number of patients who require repeat interventions due to restenosis currently sits at 2-3% [38]. The increased short-term success of drug-eluting stents when compared to uncoated stents has been widely recognized [39]. Within 31 days post-implantation, drug-eluting stents are associated with significantly larger lumen sizes than bare-metal stents. In the first 6 months after the procedure drug-eluting stents result in 13.4 fewer deaths per 1000 patients than bare-metal stents [40]. Target vessel revascularization is reduced by 52-74% and the rates of myocardial infarction fall by 33-45% in the first year [41]. By preventing the proliferation of smooth muscle cells and endothelial cells into the lumen, the first 12 months after treatment of atherosclerosis using drug-eluting stents results in an overwhelming number of positive patient outcomes. However, the processes that the drugs prevent are essential for the proper healing of the artery. This is reflected in the long-term results. The delayed healing and incomplete re-endothelialization

leave the damaged section of the artery at an elevated risk for developing life-threatening thrombosis [42]. After 2 years post-procedure, mortality rates of drug-eluting stents have been found to be nearly identical to bare-metal stents, or in some cases, even higher [43] [44]. One review of patient outcomes following stent implantation found that drug-coated stents had a 7.2% risk of death versus a risk of 3.8% for an uncoated control group after 2 years. The gap in mortality rate only grew, and at 5 years was found to be 14.7% and 8.1% for coated and uncoated stents respectively [45].

2.6 Nanovesicles as a Treatment Method

A new and promising treatment method that has garnered interest from the medical community is the use of extracellular vesicles. Certain extracellular vesicles have been found to promote tissue regeneration [46]. These vesicles are part of the natural healing process that the human body undergoes when there is tissue damage. This has led to the hypothesis that extracellular vesicles, rather than drugs, should be used to coat stents before implantation. This hypothesis, which has only been recently developed, has yet to be tested in long-term patient outcome research. However, analyses on the potential impact of extracellular vesicle coatings have been carried out. Two separate studies, each conducted in 2021, considered the use of exosome-eluting stents. The researchers found that the exosomes were able to enhance the proliferation rate and the migratory and tube-forming capabilities of endothelial cells while impairing the migration of smooth muscle cells [47] [48]. Since ISR is commonly a result of the proliferation and migration of smooth muscle cells, which leads to significant growth of the vascular wall into the lumen, exosome-eluting stents provide a promising therapeutic approach for patients who require cardiovascular stents. In addition, they not only prevent restenosis but

by promoting endothelial cell proliferation as well as tissue regeneration, the concerns of thrombosis that are observed with drug-eluting stents are negated. Another such extracellular vesicle that is being considered for stent coatings is mesenchymal stem cell-derived nanovesicles. Researchers have been able to develop human mesenchymal stem cell-derived nanovesicles that are functionalized with the flow-targeting peptide GSPREYTSYMPH (PREY) [8]. These PREY-expressing nanovesicles (PMSC-NVs) act as an anti-inflammatory agent and promote endothelial recovery.

2.7 In Silico Stent Design

The advent of cardiovascular stenting has transformed the landscape for treating cardiovascular diseases. Doing so by providing a minimally intrusive means for restoring proper blood flow and alleviating symptoms. Stenting is not a perfect solution, and much work has gone into improving their efficacy. Changes such as the material used or adding a drug-eluting coating are methods that have been found to influence stenting's effectiveness. Another key contributor that has been identified is stent geometry. The geometry of the stent plays a very important role in the mechanical and medical success of the device. How a stent interacts with the blood and the vascular wall is heavily dependent on its design.

2.7.1 Disruptions to Blood Flow

When a stent is expanded into an artery, the outer edge of the stent, in an ideal expansion, presses against the vascular wall. The radial thickness of the stent struts means that a portion of the stent protrudes into the lumen, and thus interacts with blood flow. The laminar flow that occurs in the portions of the artery leading up to the location of the stent is suddenly

disrupted. What results are recirculation zones immediately upstream and downstream of the struts [49]. This deters vascular healing, increases platelet aggregation, and increases the chances of thrombosis [50]. In a randomized clinical trial where this phenomenon was investigated, 651 patients were assigned a stent with strut heights of either 50 µm or 140 µm. The researchers compared the success of each group by analyzing their respective rates of restenosis at 6 months. It was found that the group given the larger strut thickness experienced rates of restenosis that were nearly twice as high as the thin strut group, 25.8% and 15.0% respectively. With interventions being required in 8.6% of cases for the thin strut group and 13.8% for the thick struts [49]. This is also reflected in the outcomes of second-generation drug-eluting stents when compared to the newer ultrathin strut drug-eluting stents. The ultrathin strut, which is typically 60-65 µm tall, is associated with a 16% reduction in target lesion failure and myocardial infarction when compared to the second-generation drug-eluting stent, typically 80-90 µm tall struts [51]. In a porcine model, researchers Kolandaivelu et al. looked to investigate this problem. The researchers used stents that had strut dimensions of 81x81 µm or 162x81 µm. Apart from the height of the struts, the stents were identical. When examining the impact of this geometric feature, the researchers found that the cases where the 162 µm height was used were 49% more thrombogenic [52]. The overwhelming evidence indicates that larger struts, which lead to an increased disruption to blood flow, reduce the efficacy of cardiovascular stents. Since the disruption to flow cannot be completely negated, focus has been paid to methods that can be used to limit the detrimental effect. When the flow is interfered with, certain areas of the arterial wall will experience low wall shear stress. It is in these regions where thrombosis tends to occur. To examine methods for limiting the regions of low wall shear

stress, in-silico methods need to be used. This allows researchers an easy method for obtaining the exact values of wall shear stress of a stented arterial section. Through this technique, it has been found that the average wall shear stress decreases along the flow direction in a stented artery [53]. These results are corroborated by a clinical study where patients' rates of stent thrombosis, death, and myocardial infarction were assessed and compared to the length of the stent. It was found that patients with longer stents were at increased risk of all three outcomes and that the threshold for the elevated risk began at stents with a length above 31.5 mm [54]. Another factor affecting wall shear stress is the intrastrut angle. The larger the angle, the less the strut is aligned with the primary direction of flow. This causes larger flow disruption and larger areas of low wall shear stress. In an optimization analysis, it was found that an intrastrut angle of 40 degrees minimized the area of the vascular wall that experiences low wall shear stress [55].

2.7.2 Mechanical Loading

Another consideration that needs to be taken when optimizing stent design is the loading that the stent will experience. In its unexpanded form, the stent should be as small and flexible as possible, to safely navigate the vasculature leading up to the diseased location. During balloon expansion, the stent will plastically deform to its final diameter, reaching a shape and size where it must stay. When designing a stent, the plastic deformation and performance as well as the compression resistance must be considered. An example of this was carried out by Li et al., where a finite element analysis paired with a non-dominant sorting genetic algorithm was used to improve upon the design of a sinusoidal stent. The algorithm was used to search for optimal design solutions, and the finite element analysis was used to measure the

stresses the stent experienced during expansion and its radial strength post-expansion. During the analysis researchers did not consider the use of different materials, but only adjustments to the stent design and strut dimensions. The optimized design had struts with a 30.4% reduction in cross-section, leading to a 38.7% increase in radial strength, a reduction in axial residual stress of 50.8%, and a surface coverage that was reduced by 15.0% [56]. Another consideration is the fatigue life of the stent. The Food and Drug Administration guidelines state that a stent must be able to survive 10 years or 400 million cycles under physiological loading [57]. Failure of a stent is associated with loss of radial support of the stented vessel, thrombosis, or even damage to the artery by the fractured struts. Fatigue failure poses a significant risk to stent success, yet very little work has been done considering it during geometric design optimization [57].

2.7.3 Creating an Accurate Drug Eluting Stent Simulation

The optimization of drug-eluting stents requires objectives that are more complex than simple material failure. One such case, the investigation of which can help direct future numerical simulations as well as the design of drug-eluting coatings, is flow-mediated drug uptake. Researchers have found that the depletion at surfaces exposed to blood flow is too great for there to be any significant uptake of the drug from the blood into the vasculature [58]. For drug-eluting stent design purposes, this indicates that applying a coating to all sides of the stent does not provide any more benefit than simply coating the sections that contact the arterial wall. In addition, the modeling of drug elution directly into the lumen off the scaffold can be neglected, reducing the computational load while continuing to provide accurate results of in-silico analyses. Unlike flow-mediated drug uptake, assuming blood as a Newtonian fluid is

not a simplification that can be made. When comparing equal simulations of drug-eluting stents, the cases where the Newtonian fluid assumption is made incorrectly result in significantly lower concentrations of drug in the artery [59]. Similar conclusions are reached when comparing steady state conditions to transient conditions. Under steady state conditions, the blood velocity is constant and the release of the drug off the stent is also unchanging. In the transient, case blood flow is pulsatile and the store of the drug on the stent depletes, leading to a gradual reduction in elution over time. The steady state case is found to greatly overestimate both the drug concentration in the artery as well as the uniformity of the drug distribution [58] [60]. This plays an important role when it comes time to evaluate the efficacy of various drug-eluting stent designs. The concentration of the drug in the artery must reach its therapeutic threshold in order to take effect, but it has also been found that the uniformity of the drug delivery is a key factor [61] [62]. A stent that provides a more even distribution will have higher rates of positive patient outcomes [62]. It is for this reason that drug distribution needs to be considered when evaluating stent design.

2.7.4 Drug-Eluting Stent Optimization

When analysing stent design, a general geometric configuration is normally used with certain parameters being varied. The results are typically only applicable to the design selected. However, in certain instances, specific results can be found that reach much broader applications. In two papers, published in consecutive years, Pant et al. did exactly that. The researchers used the length of the stent, the spacing between struts, and the width of each strut as parameters. An optimization analysis took place with objective functions of recoil, volume average stress, flexibility, and drug concentration. The expansion of the designs was

assessed using ABAQUS/Explicit 6.9.1, a finite element solver, and the hemodynamics and drug distribution were evaluated using Star-CCM+, a computational fluid dynamics (CFD) solver. In both studies, the drug concentration, recoil, and average stress objectives favored larger stents with larger surface areas. Upon further analysis of the drug distribution, the researchers remarked on an interesting result. The designs with the largest surface areas resulted in a higher concentration of drug in the artery, but the uniformity of the distribution was worse [63] [64]. The researchers found that average drug concentration and the uniformity of the distribution were inversely correlated. As a result, the researchers concluded that the optimal design, when only considering the drug-elution of the stent, would have a minimal surface area that would still allow the therapeutic concentration threshold to be met. In this way, the eluted drug still has the proper impact on the artery, but its distribution is as uniform as possible to promote optimal healing.

3.0 Methods

3.1 Blood Flow Biomechanics

3.1.1 Properties

Blood is composed of erythrocytes, leucocytes, and platelets suspended in plasma. On average, blood is composed of 55% plasma [65]. The other 45%, which represents the corpuscles, is known as the hematocrit. The hematocrit level plays a significant role in defining the properties of blood. For this experiment, blood was modeled with a hematocrit of 45%. Blood density is constant and was set as 1060 kg/m^3.

The complex construction of blood leaves it with unique rheological properties. Characterized by shear thinning behaviour, blood is not a Newtonian fluid. To improve accuracy, a non-Newtonian model must be used, especially when modeling drug-eluting stents, as described by Song et al. (2021). The researchers found that a simulation using a Newtonian model drastically underpredicts the drug concentration in the artery [59]. The Carreau model, which can accurately represent blood viscosity across a wide range of shear rates, was chosen as the viscosity model.

3.1.2 Governing Equations

To define the basic equations that govern blood flow, several assumptions were made. The first is that the flow leading up to the modeled arterial section is fully developed, incompressible, and laminar. Another necessary assumption is that the artery is treated as a rigid wall. By doing so structural equations can be neglected, and only the fluid equations need to be considered. A study conducted by Berry et al. (2000) validates this assumption. In their analysis, the researchers found that the diameter of a stented section of an artery experienced diameter changes of less than 2% [66].

Based on the assumptions stated above, the two conservation equations of mass and momentum must be solved to fully describe the blood flow. To do so, the CFD software must define and solve the mass conservation equation and the momentum conservation equation. The conservation of mass equation can be written as:

$$\frac{\partial \rho}{\partial t} + \nabla \cdot (\rho \vec{v}) = S_m \tag{1}$$

The first term, $\frac{\partial \rho}{\partial t}$, is the time rate of change of density. The incompressible assumption means that blood density is unchanging, and thus, $\frac{\partial \rho}{\partial t} = 0$. Similarly, S_m, which is defined as the mass added to the continuous phase from the dispersed second phase is also zero. The vector $\vec{v}$ is the local velocity and has units m/s. Therefore, we are left with the final version of the conservation of mass equation:

$$\nabla \cdot (\rho \vec{v}) = 0 \tag{2}$$

The momentum equation that is solved by Fluent for an inertial reference frame is:

$$\rho \left(\frac{du}{dt} + u \cdot \nabla u \right) = -\nabla \rho + \nabla \cdot \tau + \rho g \tag{3}$$

The stress tensor τ, is defined as:

$$\tau = -\eta(\dot{\gamma}) \cdot (\nabla u + (\nabla u)^T) \tag{4}$$

Where $\eta(\dot{\gamma})$ is the apparent viscosity as a function of the shear rate and is defined by the Carreau model equation:

$$\eta(\dot{\gamma}) = \eta_\infty + (\eta_0 - \eta_\infty) * (1 + (\lambda \dot{\gamma})^2)^{\frac{n-1}{2}} \tag{5}$$

Here, η_∞ is the viscosity at an infinite shear rate. With a hematocrit of 45%, $\eta_\infty = 0.0345\ P$. The viscosity at zero shear rate is represented by η_0, and was set to $\eta_0 = 1.610\ P$. λ is the characteristic time, which is the reciprocal of the relaxation time and is 39.418 s. The shear rate $\dot{\gamma}$ is not a constant and is the result of the forces experienced by the fluid during flow. Lastly, n is the power law index, and was given the value of 0.479. Having a power law index that is less than one indicates that the fluid being described displays shear-thinning behaviour. The values

used for the constants of the Carreau model equation for 45% hematocrit were taken from the study by Kwon et al. (2008) [67]. The researchers used curve fitting to determine the coefficient values from experimental measurements relating viscosity and shear rate of blood at various hematocrit percentages.

3.1.3 Velocity Waveform

Blood flow through the modeled section of the artery was considered fully developed with the flow at the inlet assumed to be following a Poiseuille distribution. The following formula represents the velocity profile:

$$u(r,t) = U_{max}(1 - \frac{r^2}{R^2}) \quad (6)$$

The instantaneous velocity, u, can be determined at any point at a given radius, r. The maximum instantaneous velocity, U_{max}, is measured in m/s. The value of maximum instantaneous velocity in a stented arterial section ranges from 0.28-0.79 m/s [68]. In this study, a value of U_{max} = 0.4 m/s was selected. To determine the sensitivity of the simulation to the inlet velocity, one case was run with an inlet velocity of 0.4 m/s, and another was run with an inlet velocity of 0.8 m/s. When doubling the magnitude of the velocity, the inlet velocity, the impact on the particle concentration distribution in the arterial wall was found to be negligible. R is the radius of the artery in meters. For this study, the radius is set to 0.00175 m.

To accurately model pulsatility, the 3D paraboloid at the inlet surface, which is defined by (6), is multiplied by a time curve that is representative of the physiological waveform of blood flow. A triphasic waveform, displayed in Figure 2 below, was selected that includes backward flow for 3% of each pulse. The exact waveform displayed is what was used to scale the inlet velocity. A

similar waveform was used by Feldman et al. (2002) in their computational analysis of blood flow through the human coronary arteries [69]. The following waveform correlates to a heart rate of approximately 70 beats per minute:

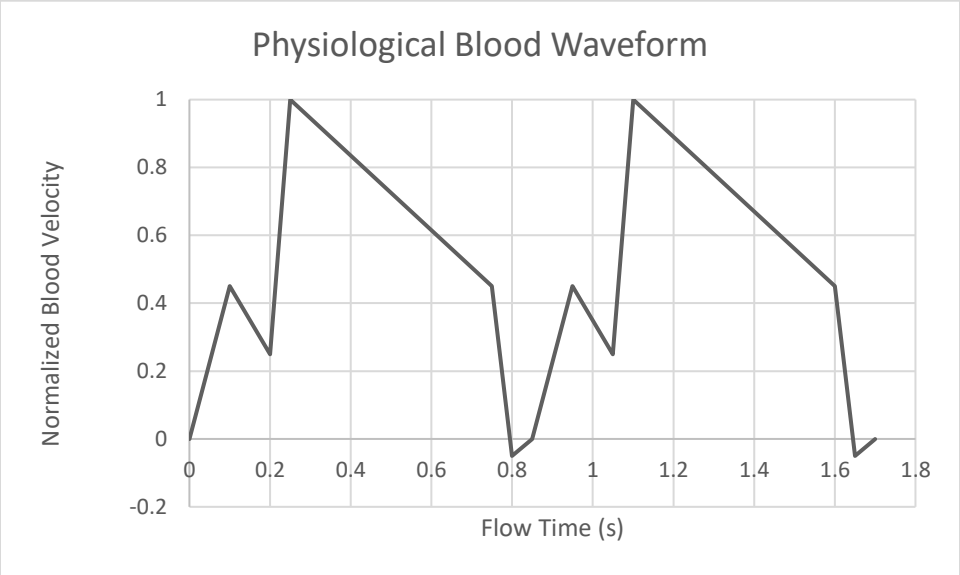

Figure 2: Normalized velocity waveform used to model pulsatile blood flow. Adapted from [69].

3.2 Nanovesicle Diffusion

The nanovesicle diffusion off the stent and into the artery was modeled using a user-defined scalar (UDS) transport equation. For single-phase flow, ANSYS Fluent solves the following equation for an arbitrary scalar ϕ_k:

$$\frac{\partial \rho \phi_k}{\partial t} + \frac{\partial}{\partial x_i}\left(\rho u_i \phi_k - \Gamma_k \frac{\partial \phi_k}{\partial x_i}\right) = S_{\phi_k} \; k = 1, \ldots, N \tag{7}$$

The diffusion coefficient, Γ_k, and the source term, S_{ϕ_k}, are determined by user inputs for each of the N scalar equations. The diffusion coefficient was one of the parameters analysed in this study, and thus, a range was explored. The exact diffusion coefficient of the PMSC-NVs, detailed

by Yoon et al. (2020) as a potential therapeutic agent to promote vascular healing post-stenting, is yet to be identified. A reason for the optimism surrounding PMSC-NVs is because of their similarity in structure and behaviour to naturally occurring extracellular vesicles, such as exosomes. In the study by Yoon et al. (2020), the researchers detail the process of producing the PMSC-NVs, and state that the average diameter was 47.2 ± 12.1 nm [8]. With this information, Figure 3 was used to approximate the diffusion coefficient of the PMSC-NVS based on the diffusion coefficient of an equivalent exosome in the extra-cellular environment.

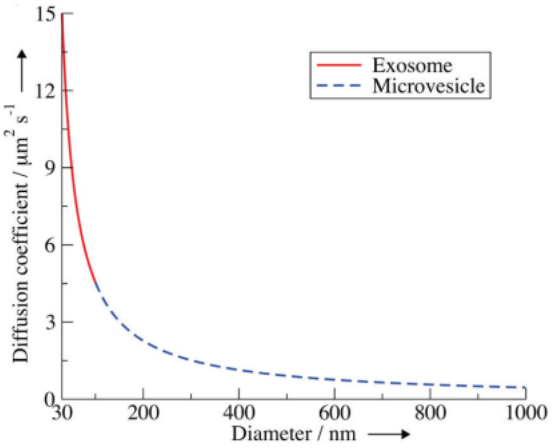

Figure 3: Diffusion coefficient vs diameter of exosomes and microvesicles [70].

With an average diameter of 47.2 nm, an exosome would have a diffusion coefficient of approximately $5.5 \cdot 10^{-12}$ m²/s in the extracellular environment. This value is an estimation of the possible value for the diffusion coefficient of the PMSC-NVS in the artery wall, but further experimental work is required to determine the proper value. Due to the uncertainty caused by the lack of experimental testing, a physically viable range of three decades above and below the literature value was explored. The total list of diffusion coefficients and material diffusivities analysed are shown below in Table 1. The vascular tissue is stagnant, and thus, the movement

of the nanovesicles throughout the artery wall is entirely controlled by diffusion. The blood, however, is not stagnant. The transportation of the nanovesicles through the blood is dominated by the blood flow. Consequently, the diffusion of particles in the blood will negligibly influence the particle motion and concentration distribution homogeneity in the artery wall.

Table 1: Diffusion coefficients and the corresponding artery and blood UDS diffusivities explored.

Diffusion Coefficient in Extracellular Material $(\frac{m^2}{s})$	**Artery UDS Diffusivity** $(\frac{kg}{m \cdot s})$
$5.5 \cdot 10^{-15}$	$7.15 \cdot 10^{-12}$
$5.5 \cdot 10^{-14}$	$7.15 \cdot 10^{-11}$
$5.5 \cdot 10^{-13}$	$7.15 \cdot 10^{-10}$
$5.5 \cdot 10^{-12}$	$7.15 \cdot 10^{-9}$
$5.5 \cdot 10^{-11}$	$7.15 \cdot 10^{-8}$
$5.5 \cdot 10^{-10}$	$7.15 \cdot 10^{-7}$
$5.5 \cdot 10^{-9}$	$7.15 \cdot 10^{-6}$

For each of the three simulation studies investigated, the nanovesicle diffusion was handled differently. The amount of diffusion was defined by a flux off the surface of the stent apposed to the vascular wall. The three studies are steady state, six-second transient, and 14-day transient. Both the steady state and six-second transient simulations had steady flux. In the six-second transient simulation, the time scale is so short, that the store of nanovesicles coated onto the

stent would not observe significant depletion, and thus, the flux would be insignificantly affected. For the 14-day and steady state simulations, the maximum flux was set to $1.0\ (\frac{kg}{m^3} \cdot \frac{np}{m^2 s})$. There are yet to be any experimental results that would influence this value, so, $1.0\ (\frac{kg}{m^3} \cdot \frac{np}{m^2 s})$ was selected because it is easily scalable, allowing the results obtained in this study to be adjusted once experimental testing is completed. However, for the six-second simulation, this flux was too low for there to be observable and significant results. Instead, the six-second simulation had its flux scaled by a factor of ten to $10.0\ (\frac{kg}{m^3} \cdot \frac{np}{m^2 s})$. Unlike the six-second and steady state case, the 14-day transient simulation must model nanovesicle depletion on the stent. The depletion was modeled as an exponential decrease in flux. The rate of which was defined based on conversations with Dotter Inc. (Seoul, Republic of Korea). The time-varying flux is shown below in Figure 4. The depletion model is described in more detail in the 14-day transient simulation study section below. To determine the influence of the random selection of particle flux magnitudes, an analysis was conducted where a simulation study with a flux magnitude of $7.0\ \left(\frac{kg}{m^3} \cdot \frac{np}{m^2 s}\right)$ was compared to the results of the steady state study. Increasing the flux led to a significant increase in particle concentration in the artery wall, but even when increasing the particle flux seven times, the trends of particle distribution uniformity were identical to the cases where a flux of $1.0\ (\frac{kg}{m^3} \cdot \frac{np}{m^2 s})$ was used.

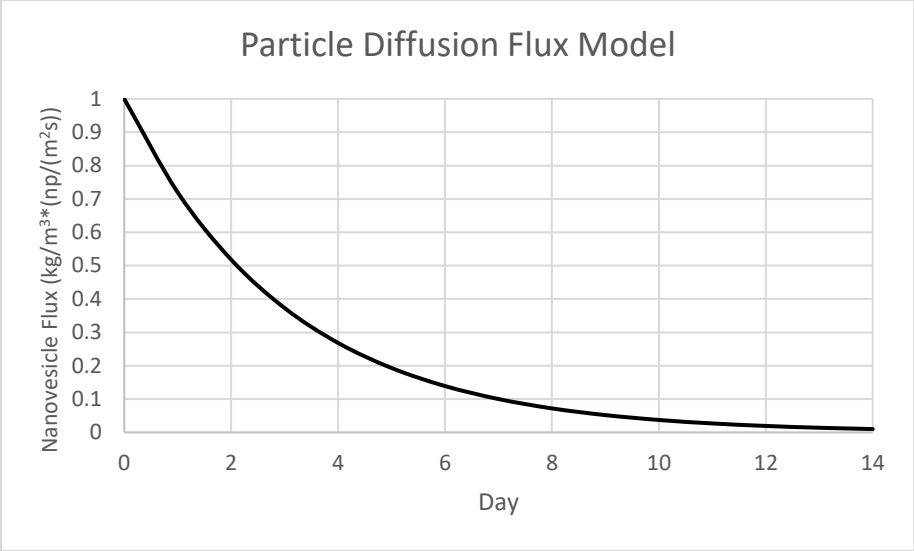

Figure 4: Time-dependent nanovesicle flux for the 14-day transient simulation.

3.3 Computational Domain and Simulation Setup

3.3.1 Stent Geometry

In total, 11 different stent geometries were created and analysed in this study. The differences in the designs between all 11 cases are variations of a base stent design provided by Dotter Inc. (Seoul, Public of Korea). The basic design is displayed in its expanded form in Figure 5 and its flat pattern in Figure 6. The stent is a slotted-tube design with repeating closed cells in alternating directions. There are 16 columns of trapezoidal-shaped cells that alternate in direction and are offset by half a cell between each column. On the ends are arrow-shaped cells, which are much larger than the trapezoidal cells. The columns of arrow cells point in opposite directions. In each column of cells, there are six cell units. The design is symmetrical, and the red line running longitudinally along the struts in Figure 5 displays the symmetry plane. Only half the stent needed to be modeled due to this symmetry.

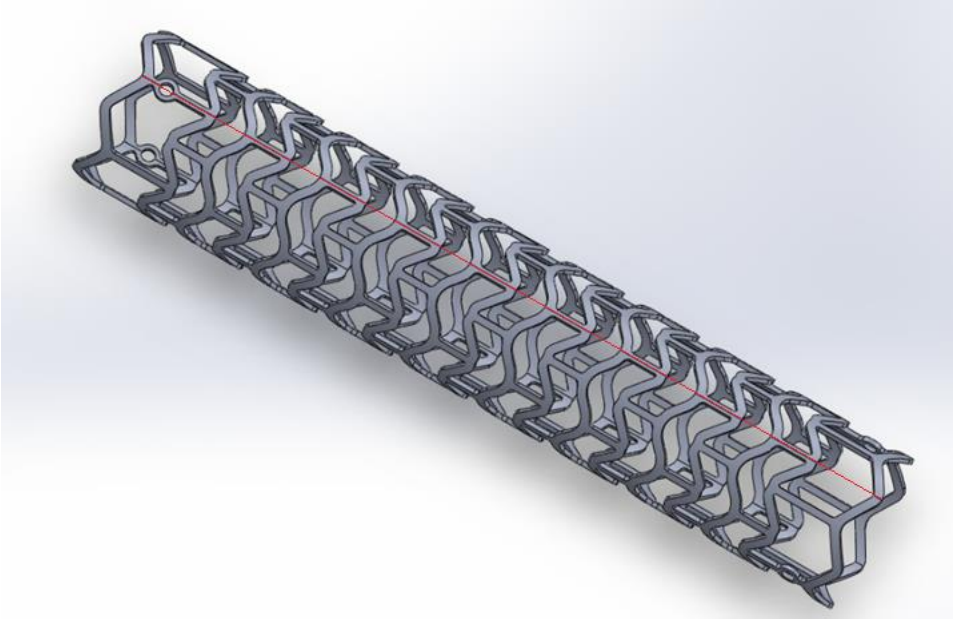

Figure 5: 3D geometry of Dotter Inc. (Seoul, Republic of Korea) stent. The symmetry plane is indicated by the red line.

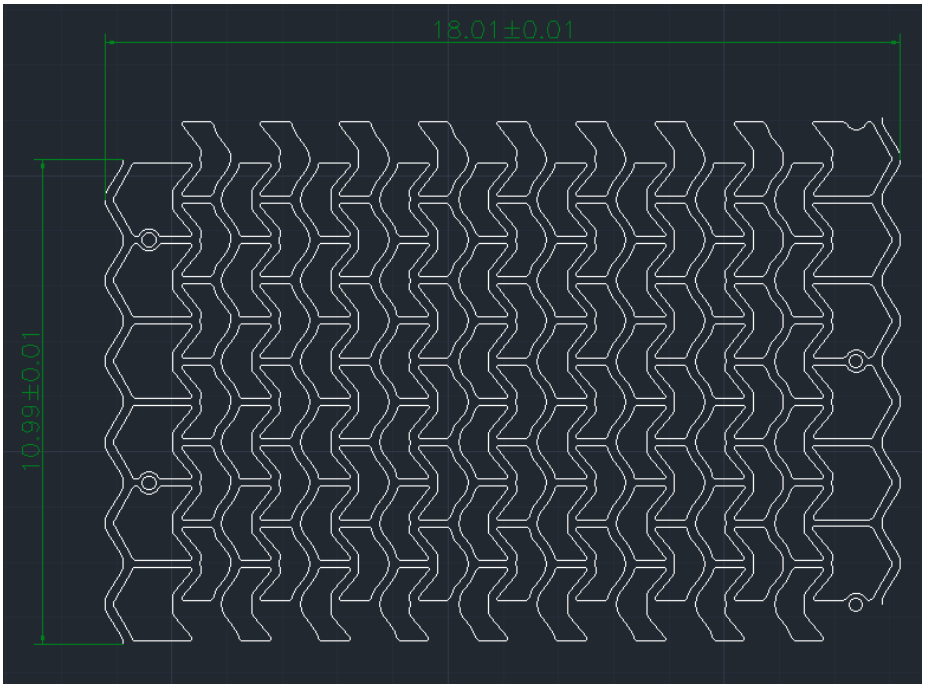

Figure 6: Flat pattern of Dotter Inc. (Seoul, Republic of Korea) stent.

Alterations made to the geometry of the stent were done by adjusting the size of the cells. An offset was created to either increase or decrease the size of each of the cells. An example of creating the offset is displayed in Figure 7.

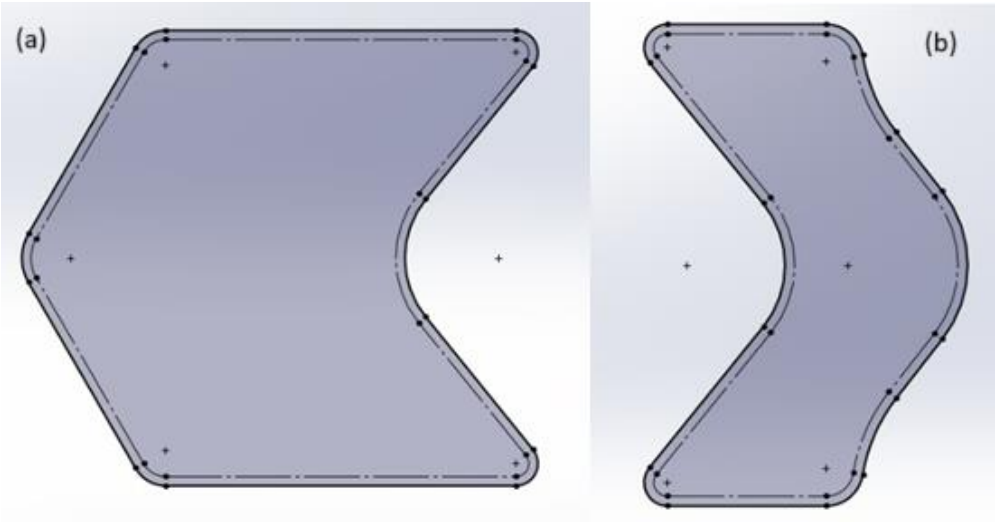

Figure 7: Example of offsets used to create larger arrow cells, (a), and trapezoid cells (b). The dashed lines are the original cell geometry, and the solid lines are the new cell geometries after applying the offset.

The geometries created and analysed are displayed in Table 2. A positive offset, which increases the size of each cell, causes a reduction in the outer surface area of the stent, with a negative offset having the opposite effect. The designs with the largest offsets are presented in Figure 8.

Table 2: Cell offsets, strut widths, and corresponding half-stent outer surface area for each of the 11 geometries.

Offset (mm)	Strut Width (mm)	Half Stent Outer Surface Area (mm^2)
0.035	0.09-0.13	20.267
0.020	0.12-0.15	24.779
0.015	0.13-0.16	26.260
0.010	0.14-0.17	27.732
0.005	0.15-0.19	29.207
0.000	0.16-0.20	30.664
-0.005	0.17-0.21	32.117
-0.010	0.18-0.22	33.561
-0.015	0.19-0.23	35.000
-0.02	0.20-0.24	36.425
-0.035	0.23-0.27	40.657

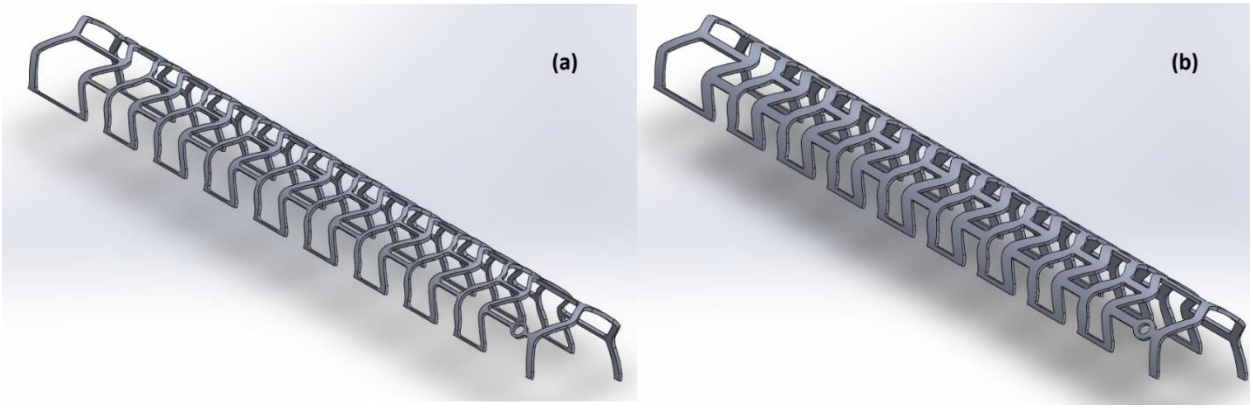

Figure 8: The half stent with its smallest, (a), and largest, (b), surface areas

3.3.2 Stent, Artery, and Lumen

To complete the 3D model, the lumen and artery were created. Identical to the stent geometry, only half of the lumen and artery were generated. The lumen was modeled as a half cylinder, with a diameter that is the same as the outer diameter of the stent, 0.0035 m. In this way, the simulation was completed with the outer surface of the stent fully apposed to the arterial wall. The artery was built around the stent and lumen with a thickness of 0.5 mm, a typical thickness for healthy arteries post-stenting [71]. The artery, stent, and lumen geometry are displayed below in Figure 9. The geometry was configured so that the z-axis runs along the longitudinal direction of the lumen and artery, the dashed line in Figure 9 (a). The x-axis runs parallel to the symmetry plane. In Figure 9, this is along the direction of the flat edge of the semi-circle created by the symmetry plane. The y-axis is perpendicular to the symmetry plane, pointing upward through the lumen and into the artery.

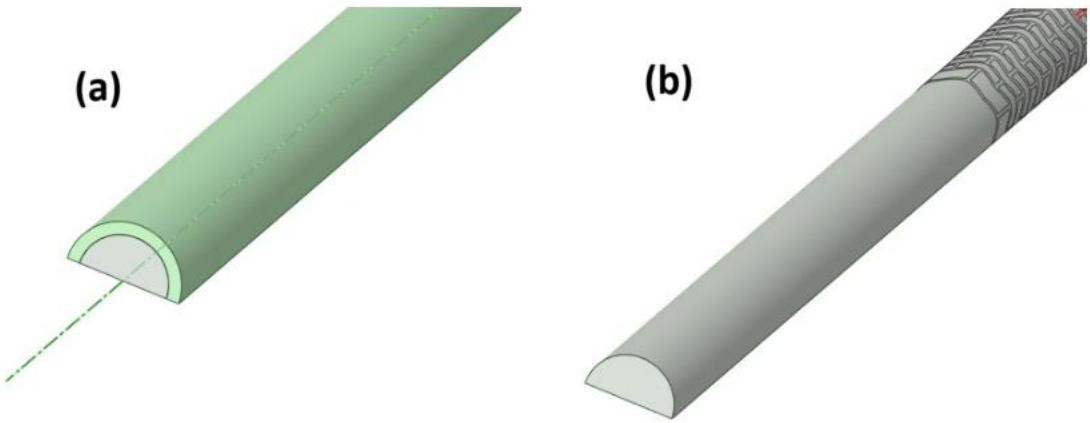

Figure 9: The modeling of the artery and the lumen. In (a), the artery (green) and lumen (grey) are displayed. In (b) the artery has been removed and the top of the stent can be seen.

3.3.4 Mesh

The 3D mesh was generated using Fluent Meshing. To ensure a proper mesh size, a grid independence analysis was conducted. Meshes with differing levels of complexity were created and tested. A trial was run for each mesh to determine the steady state particle concentration in the artery. The outcome of such an analysis is to determine the mesh of minimal complexity where further refinement does not provide any significant increase in simulation accuracy. The mesh that achieved independence was a tetrahedral volume mesh with 2.5 million cells. When the number of cells was doubled to nearly 5 million, the average particle concentration in the artery changed by only 0.64%. Doubling the mesh refinement results in a less than 1% change in results, indicating independence had been reached. This mesh size is comparable to the sizing used in similar work, done by Chen et al., where the researchers conducted eluting stent simulations using a mesh size of 1.8 million cells [53].

A 3D mesh was created for both the lumen and artery volumes, but only the surface of the stent was modeled. The particles, which eluted off the vascular-facing surfaces of the stent, cannot enter the interior of the struts. As a result, modeling the interior of the stent would be unnecessary and needlessly increase the computational load.

Inflation layers were created at the vascular wall and the edges of the stent struts to allow for accurate modeling of the complex fluid and particle behaviour in these regions without significantly increasing the computational load. The arterial wall was set as a coupled boundary. This condition was selected so that the wall is treated as an interface between two regions. In this case, it is the interface between the lumen and the artery. A typical resulting mesh is shown below in Figure 10.

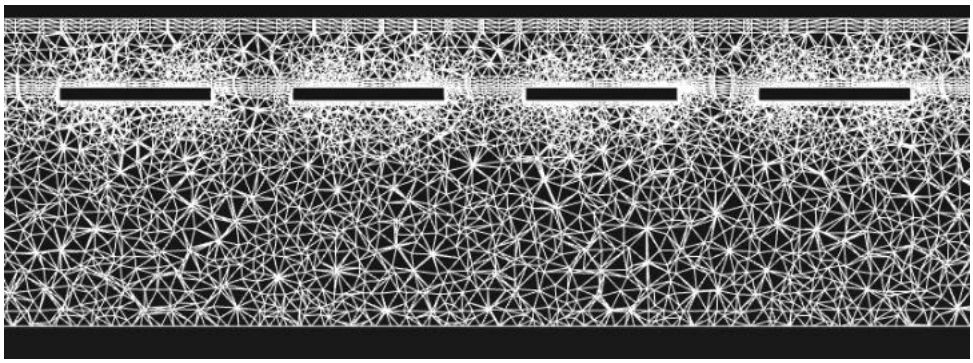

Figure 10: Longitudinal cross-section of the 3D tetrahedral mesh that achieved independence. The empty black rectangles are the interior of the stent struts that were not meshed.

3.3.5 Temporal Resolution Independence

Another factor that can influence the accuracy of an in-silico study is the size of the time step. For time-dependent simulations, a proper time step must be used to prevent divergence of results. At each timestep, the solver is performing an approximation. As the time step grows, so does the size of this approximation, until a point is reached where the simulated results no longer accurately represent what is being modeled. The smaller the time step, the more accurate the approximation, but the computational time to run the simulation increases. A compromise needs to be made where the largest time step that still allows for accurate results is identified. To determine this point, an independence analysis can be conducted, similar to the analysis conducted for the mesh sizing. The average particle concentration over a surface of 0.1 mm from the vascular wall in the radial direction was selected. Time steps of 1, 0.5, 0.1, and 0.05 seconds were evaluated. The results are displayed in Table 3 below. From the analysis, a time step of 0.1 seconds was selected. When the time step was halved from 0.1 to 0.05 seconds, the results changed by only 5.0%.

Table 3: Results from the time step independence analysis.

Time Step	Surface Average UDS Scalar
1 second	0.0083580697
0.5 seconds	0. 006524598
0.1 seconds	0.005515511
0.05 seconds	0. 0052388507

3.3.6 Test Matrix and Optimization Objectives

A total of three separate simulation studies were created and tested. For each, the same parametric analysis was conducted using the 77 combinations of cell offsets and diffusion coefficients. The distinction between the studies is marked by the inlet velocity and nanovesicle flux, as detailed in Table 4. The three studies are a steady state analysis, a six-second transient analysis, and a 14-day transient analysis. In the artery, four lines and four surfaces of constant radius were created. The surfaces and lines were at depths in the artery radially from the vascular wall of 0.1 mm, 0.2 mm, 0.3 mm, and 0.4 mm. The concentration and uniformity of the nanovesicle distribution were evaluated at these surfaces. Uniformity was determined as the root mean square error (RMSE) of the nanovesicle measurements along each radial surface normalized by their respective mean. The formula for calculating RMSE is displayed below in (8). The value n is the number of observations, y_i are all the observed values of the particle density on the surface, and $\bar{y}$ is the average particle density on the surface. The values of RMSE for each design point were then normalized by the maximum RMSE value found on the same surface for the same simulation case.

$$RMSE = \sqrt{\frac{\sum_{i=1}^{n} (\frac{y_i}{\bar{y}} - 1)^2}{n}} \quad (8)$$

3.3.6.1 Steady state

A steady state analysis is defined by its time independence. Rather than solving for changes to the system over a time step, the software solves for the equilibrium conditions. To do so, there can be no time variation in the input parameters. For this study, those factors are the nanovesicle flux off the stent and the inlet blood velocity. Pulsatility is ignored and the inlet flow is assumed to be fully developed and unchanging. Similarly, the depletion of nanovesicles in the stent coating is also disregarded. The result of which, is a steady flux of nanovesicles into the artery.

3.3.6.2 Short Term Transient

At a heart rate of 70 beats per minute, seven heartbeats can be simulated in six seconds. The purpose of this simulation case is to determine the short-term time dependence of the nanovesicle uniformity in the artery. The short timescale allows for accurate modeling of blood pulsatility. Due to this, the velocity of blood flow at the inlet in this simulation case is not constant. Instead, it is defined so that it follows the physiological waveform displayed in Figure 2. The timescale that lends itself to transient blood flow also results in steady nanovesicle flux. The diffusion of nanovesicles out of the stent coating and into the artery is largely driven by a concentration gradient that will experience a negligible reduction in six seconds. As a result, the nanovesicle flux is constant.

3.3.6.3 Long Term Transient

The therapeutic effect of the nanovesicles lasts for 14 days after stent implantation. As a result, the intended flux of nanovesicles off the stent is constructed so that the diffusion is negligible by the 14th day. The third simulation case models this process. Starting with a value of $1.0\ (\frac{kg}{m^3} \cdot \frac{np}{m^2 s})$ at day zero, the flux exponentially decreases following the formula:

$$Flux = e^{\left(\frac{-t}{3.0400614}\right)} \tag{9}$$

In (9), t has units of days. By day 14, the flux becomes $0.01\ (\frac{kg}{m^3} \cdot \frac{np}{m^2 s})$, a reduction in the flux by 100 times. At such a timescale, simplifications must be made to reduce the computational load of the simulation. The first is the time step. The time step analysis concluded that independence is achieved with a step size of 0.1 seconds. With a step of this size, it would take over 1.2 million time steps to reach 14 days. Instead, the step size was inflated so that the 14-day mark could be reached in 45 steps. The second is the blood velocity. The physiological waveform used in the six-second transient simulation is not suitable for 14 days. A steady velocity profile, identical to the blood flow modeled in the steady state simulation, was used instead.

A summary of the three simulations as well as the distinctions between them is displayed below in Table 4.

Table 4: Summary of blood flow and nanovesicle flux of the three simulation studies.

Study:	**Blood Flow**	**Nanovesicle Flux**
Steady state	Steady. Defined by (6)	Steady. $1.0\ (\frac{kg}{m^3} \cdot \frac{np}{m^2 s})$
Six Second Transient	Follows a physiological waveform where (6) is multiplied by the line plotted in Figure 2	Steady. $10.0\ (\frac{kg}{m^3} \cdot \frac{np}{m^2 s})$
14-Day Transient	Steady. Defined by (6)	Exponentially decreasing. $1.0\ \left(\frac{kg}{m^3} \cdot \frac{np}{m^2 s}\right)$ multiplied by (9)

3.3.7 Boundary Conditions

The following boundary conditions were applied:

Inlet: Longitudinal velocity (u_z) was assumed to follow a Poiseuille distribution defined by (6). In the six-second transient case, it was set to vary with time according to the physiological waveform displayed in Figure 2. The velocities in the radial directions (u_x and u_y) were set to zero at the inlet surface.

Arterial wall and stent struts: The no-slip boundary condition was applied to these surfaces. As a result, the velocity on these surfaces is zero. The artery wall is set as a coupled boundary. The nanovesicle diffusion was defined as a flux off the outer surface of the stent. In the steady state case and 14-day transient case, this was set to a value of $1.0\ (\frac{kg}{m^3} \cdot \frac{np}{m^2 s})$, with the 14-day transient case following the depletion model (9). The six-second transient case used a constant flux of $10.0\ (\frac{kg}{m^3} \cdot \frac{np}{m^2 s})$.

Outlet: The pressure at the outlet was set to zero.

4.0 Results

The particle concentration was tracked along surfaces of constant radial coordinates to determine the distribution of the eluted particles in the artery. The surfaces and their relation to the lumen are displayed below in Figure 11.

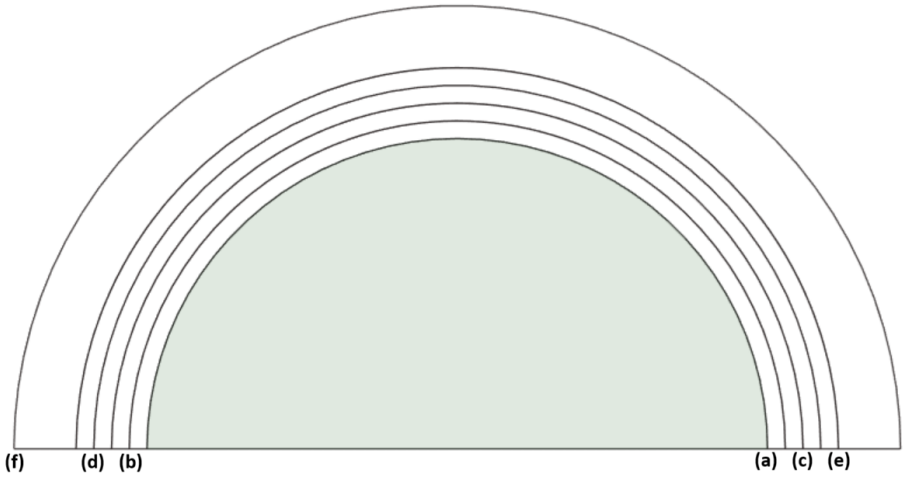

Figure 11: Outline of the edges of each surface in the model. (a) is the vascular wall, (b) is the 0.1 mm radial surface, (c) is the 0.2 mm radial surface, (d) is the 0.3 mm radial surface, (e) is the 0.4 mm radial surface, (f) is the outer arterial wall. The green hemisphere is the lumen. The white surfaces represent the vascular tissue. Surfaces (b), (c), (d), (e), and (f) are in the artery wall.

4.1 Steady state

To visualize the distribution of the nanovesicles in the artery, contours of each surface were created. The contours of the design point with an offset of 0.005 mm and a diffusion coefficient of $5.5 \cdot 10^{-12}\ {}^{m^2}/_{s}$ are shown in Figure 12. The four contours correspond to the four radial surfaces in Figure 11 above. Each contour is oriented so that blood flow travels from the bottom of the image to the top. The selected case's contours are representative of all cases

analysed, and they provide several insights into the mechanisms that control nanovesicle diffusion and distribution. The first is the impact of blood flow. The nanovesicle concentration in sections of the artery upstream and downstream of the stent displays a bias for the direction of flow. The sections downstream of the stent have higher concentrations than those upstream. The second is the dispersion of the nanovesicles at different distances from the lumen. On the 0.1 mm surface, the particle distribution takes the shape of the stent geometry, with the locations of struts and open cells being clearly visible. As the distance from the lumen grows, the exact shape of the stent is lost and the transition between regions directly above struts and those directly above open cells becomes gradual.

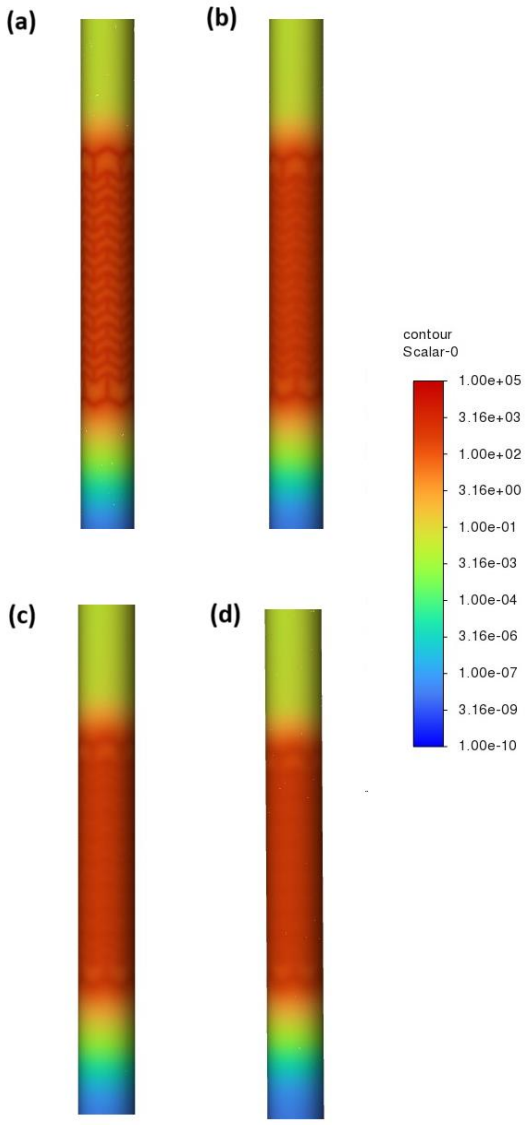

Figure 12: Contours of particle distribution in the artery at 0.1 mm, (a), 0.2 mm, (b), 0.3 mm, (c), and 0.4 mm, (d), distances radially from the lumen

Graphs were created of the nanovesicle distribution along four lines within the artery. Each line runs along the z-direction with a constant x and y value. For each line, the y-value differed, as this was the method used to control their distance from the arterial wall. All the lines had an x-value of zero. The result is that the lines only travel along the y-z plane. This correlates to the

center of the geometry concerning the x-direction. The nanovesicle distribution along these lines is plotted in Figures 13, 14, 15, and 16 below. For each case, the points along each line are assigned a colour that indicates their depth into the artery. In the model, the stented region exists between the z-coordinates -0.01 m to 0.01 m. This is evident in the graphs below, as the particle values sharply decline at -0.01 m and 0.01 m. Along each graph is a series of peaks and valleys. These points along the z-axis correlate to locations of the artery that are directly above a strut or an open cell respectively. As the depth into the artery increases, the maximum point of each peak decreases and the minimum point of each valley increases. The result is that further into the artery, the distribution of the nanovesicles becomes more uniform. When comparing the graphs below, two key observations can be made. The first is that the impact of the diffusion coefficient appears to be negligible. Plots with the same offset, but with the largest and smallest diffusion coefficients analysed are identical. Unlike the diffusion coefficient, the impact of the cell offset is apparent. The particle density in the artery scales in a linear fashion with the outer stent surface area. The design point with a surface area of 20.26 mm^2 had a maximum count, as indicated by the graph in Figure 13, of approximately 1350. When the surface area was roughly doubled to 40.65 mm^2, so did the maximum count, returning a value of approximately 2500.

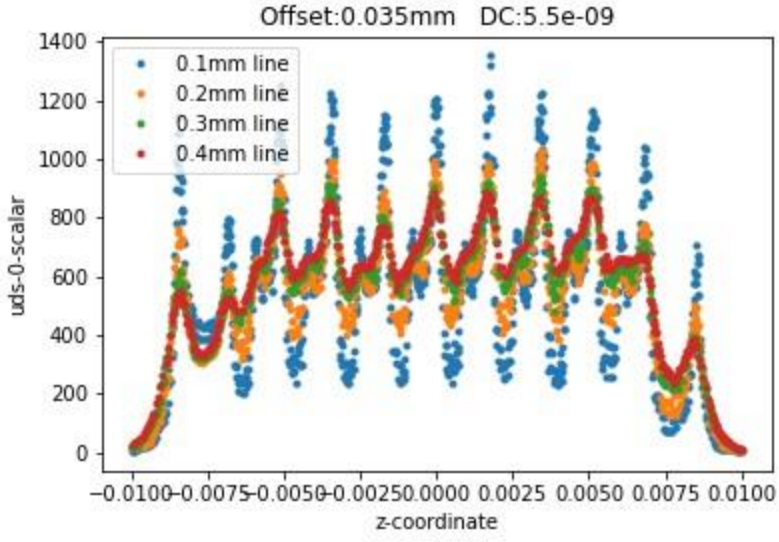

Figure 13: Particle distribution along lines in the artery for an offset of 0.035 mm and diffusion coefficient of $5.5*10^{-9}$ m^2/s

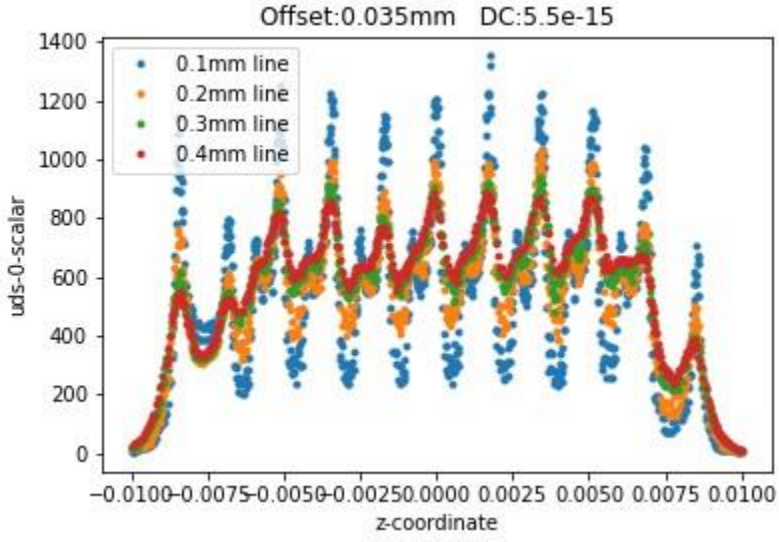

Figure 14: Particle distribution along lines in the artery for an offset of 0.035 mm and diffusion coefficient of $5.5*10^{-15}$ m^2/s

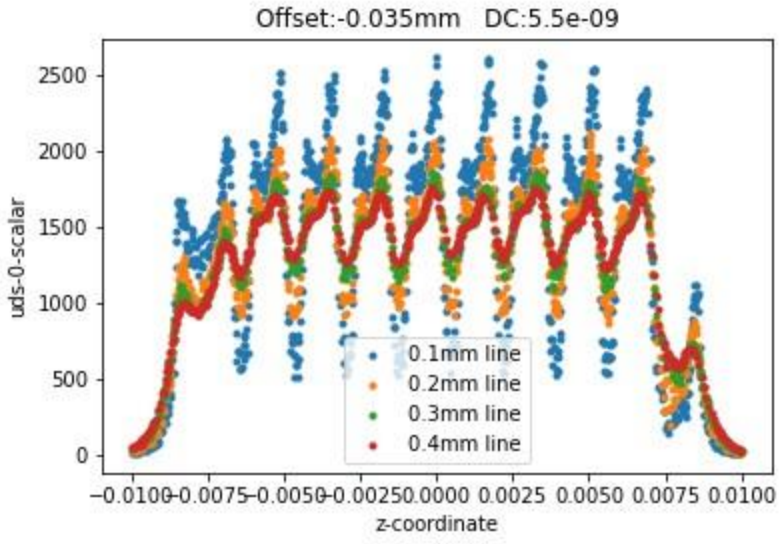

Figure 15: Particle distribution along lines in the artery for an offset of -0.035 mm and diffusion coefficient of $5.5*10^{-9}$ m^2/s

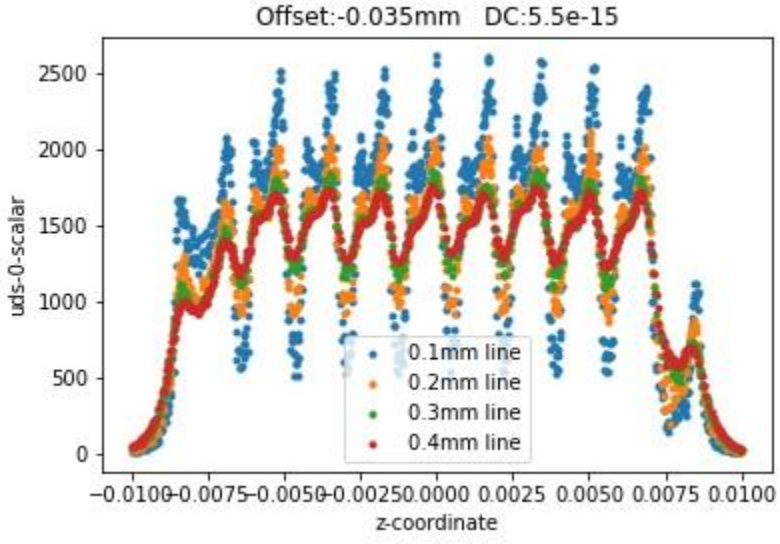

Figure 16: Particle distribution along lines in the artery for an offset of -0.035 mm and diffusion coefficient of $5.5*10^{-15}$ m^2/s

At each of the four evaluation surfaces, the variance was calculated for all 77 cases and then normalized. The results of these tabulations are shown below as four separate three-dimensional plots. The two horizontal axes are the diffusion coefficient of the particles in the arterial tissue and cell offset, and the vertical axis is the corresponding normalized variance of

each case. The minimum value of these plots, marked by a red x, indicates the case with the most uniform results. The variance values agree with the plots of the particle distribution plotted above; the diffusion coefficient does not influence the results. However, the cell offset has a pronounced effect on the nanovesicle distribution in the artery. At the surface closest to the vascular wall, at a radial distance of 0.1 mm, the most uniform case is the cell offset of -0.035 mm. This cell offset is the case with the maximum stent surface area. The trend of the plot is linear, implying a proportional relationship between the cell offset and the variance. As the cell offset shrinks, the outer surface area of the stent grows, and the uniformity of the nanovesicle distribution on the 0.1 mm surface improves. Moving further from the lumen, the plot of variance values for the surface 0.2 mm from the arterial wall is roughly parabolic. The minimum occurs at an offset of 0.01 mm. In either direction of this design point, the variance values increase. Behavior such as this signifies that the cell offset of 0.01 mm is a minimum, and exploring offsets beyond the range of those investigated in this study would only result in worse uniformity. The trend in the variation of nanovesicle distribution is the same for the 0.3 mm and 0.4 mm surfaces. For both surfaces, the relationship between cell offset and variance is approximately linear, but in the opposite direction to what is observed at the 0.1 mm surface. As the cell offset grows, the outer surface area of the stent shrinks, resulting in improved particle uniformity in the artery at radial distances of 0.3 mm and 0.4 mm from the vessel wall. Based on the trend displayed in these plots, further improvement in particle uniformity can be assumed to be made as the size of the cells grows.

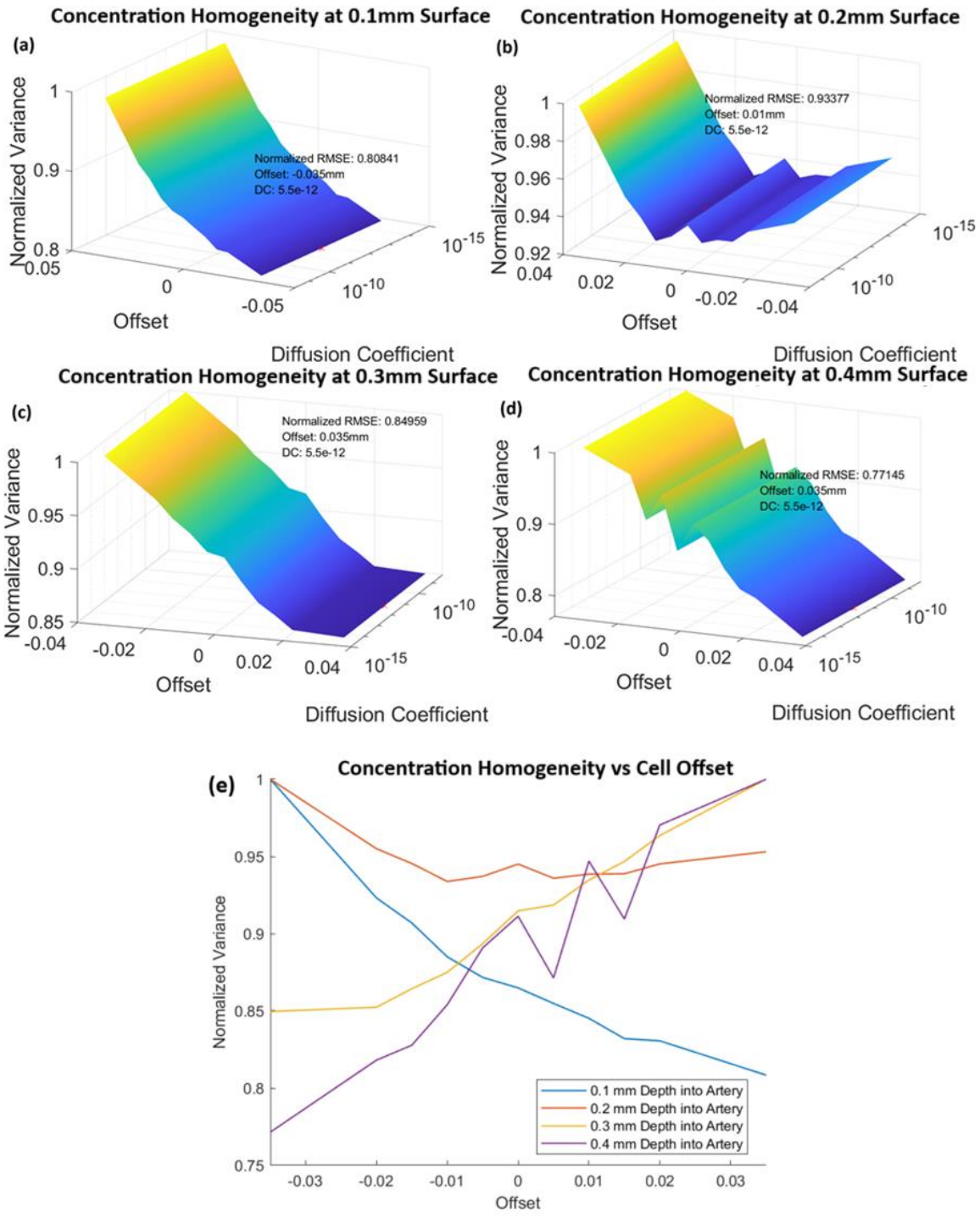

Figure 17: Variance plot for each design point at each depth into the artery. Plot (a) is 0.1 mm, (b) is 0.2 mm, (c) is 0.3 mm, and (d) is 0.4 mm. Plot (e) displays only the variance against the offset. The Offset axis direction is flipped between (a) and (b) versus (c) and (d). This is why the trends appear the same but are actually in opposite directions for (a) versus (c) and (d)

4.2 Short Term Transient

The addition of physiological flow conditions is required to produce a simulation that accurately models blood flow as well as arterial wall stresses. The changing blood velocity, including the addition of reverse flow, substantially affects the shear stresses that the vascular wall experiences. Unfortunately, improving the modeling accuracy comes at a computational cost, and the modeled timescale must be shortened to compensate. Six seconds was chosen to allow for the modeling of seven heartbeats and for the results to display the short-term dependency of particle uniformity on stent geometry and particle diffusion coefficient. To examine the potential impact of flow-mediated drug uptake, the mass average of the particles was tabulated in both the artery and the lumen. The value in the artery was consistently larger than the lumen value by a factor of 10^6. From this, it is safe to assume that the fraction of the particles that diffuse into the blood flow have a negligible effect on the particle distribution in the artery. The variance of each design point was tabulated in the same method as the steady state study, detailed in the section above. The surfaces created to display the variance for each case were made semi-transparent due to the complex nature of their shape, displayed in Figure 18 below. At each depth, the minimum point of the surface occurs at an offset of 0.01 mm and an arterial diffusion coefficient of $5.5 \cdot 10^{-12} \frac{m^2}{s}$. Though the design point with the minimum variance has a positive cell offset, the trend displays the opposite. As the cell offset becomes more negative, the particle uniformity increases. The minimum point stands as an outlier against this pattern. The designs with a negative offset, omitting the -0.015 mm offset which peaks, also display much more stable behaviour. Changes in either offset or diffusion coefficient have little to no effect on the variance of the designs in this region. The behaviour of designs

with positive offsets is much more volatile. The smallest variance occurs in this region, but, typically, so does the largest. Additionally, the diffusion coefficient greatly influences the variance of designs with positive cell offsets. The plots show that better uniformity is achieved by larger diffusion coefficients. Though the minimum variance is found in the positive offset region, changes in either offset or diffusion coefficient led to large increases in variance.

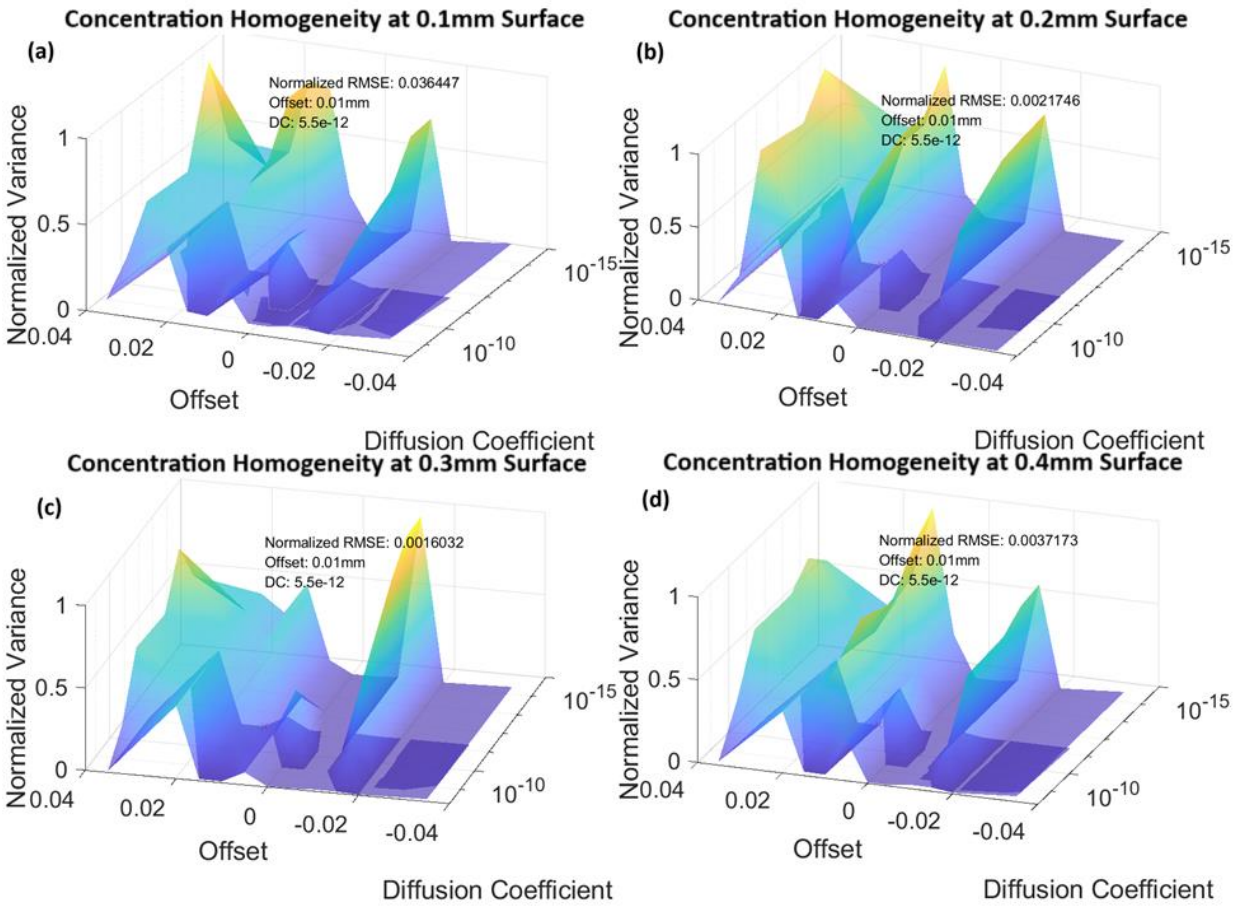

Figure 18: Variance plot for each design point at each depth into the artery after 6 seconds. Plot (a) is 0.1 mm, (b) is 0.2 mm, (c) is 0.3 mm, and (d) is 0.4 mm.

4.3 Long Term Transient

The 14-day simulation is unique due to its duration and declining nanovesicle flux. The concentration of nanovesicles within the modeled arterial section was found to exponentially increase, peak, and then exponentially decline during the duration of the simulation. The average concentration grows steadily, before peaking in the first 24 hours. At this point, the flux has dropped from a magnitude of 1.0 to 0.717 based on the defined flux model. The diffusion off the stent can no longer offset the number of nanovesicles that diffuse out of the modeled arterial section. As a result, the mass average begins to decline for the first time. The peak occurs at a mass average of roughly 700, and, by day 14, has declined to approximately 10. This behavior is graphed below in Figure 19.

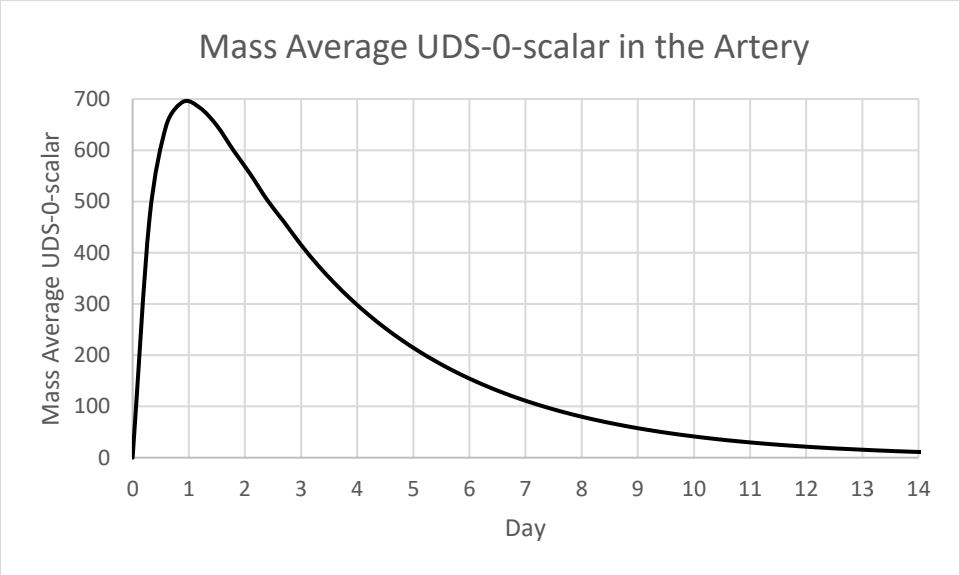

Figure 19: Average particle mass in the artery over a 14-day duration.

Though the therapeutic effect of the nanovesicles will last for 14 days, the bulk of the effect and diffusion of the nanovesicles will occur after the first three days. During this time, based on the flux model selected, nearly 64% of all the particles that will diffuse into the artery do so. After

three days, the variance, plotted in Figure 20 below, displays findings similar to the steady state simulation. The offsets that are identified for producing the highest uniformity are nearly identical to the steady state study. Unlike the steady state simulation, the diffusion coefficient greatly affects the nanovesicle distribution. The influence of the diffusion coefficient is significantly more profound than the stent geometry. When all other factors were held constant, the impact of changing the diffusion coefficient resulted in an average increase in normalized variance of 0.5. For the stent geometry, this value was only 0.05. For each of the four surfaces, the relationship between variance and diffusion coefficient takes similar shapes. At large diffusion coefficients, the variance is low. As the diffusion coefficient decreases along a log scale, the variance exponentially increases. In the case of the 0.1 mm and 0.2 mm surfaces, the variance value is still increasing at the edge of the design space. The plots of the 0.3 mm and 0.4 mm surfaces differ from the other two in this regard. Both plots display the variance value peaking, and then beginning to decline with continued shrinking of the diffusion coefficient. For the 0.3 mm surface, the decline in variance value is not significant enough to lower it beneath the value achieved with the larger diffusion coefficients on the opposing side of the peak. In the plot of the 0.4 mm surface, this does occur, and the design point with the lowest variance is the one with the lowest diffusion coefficient. The trends at the edge of both the 0.3 mm and 0.4 mm surface plots imply that the variance value may continue to decrease as the diffusion coefficient shrinks further.

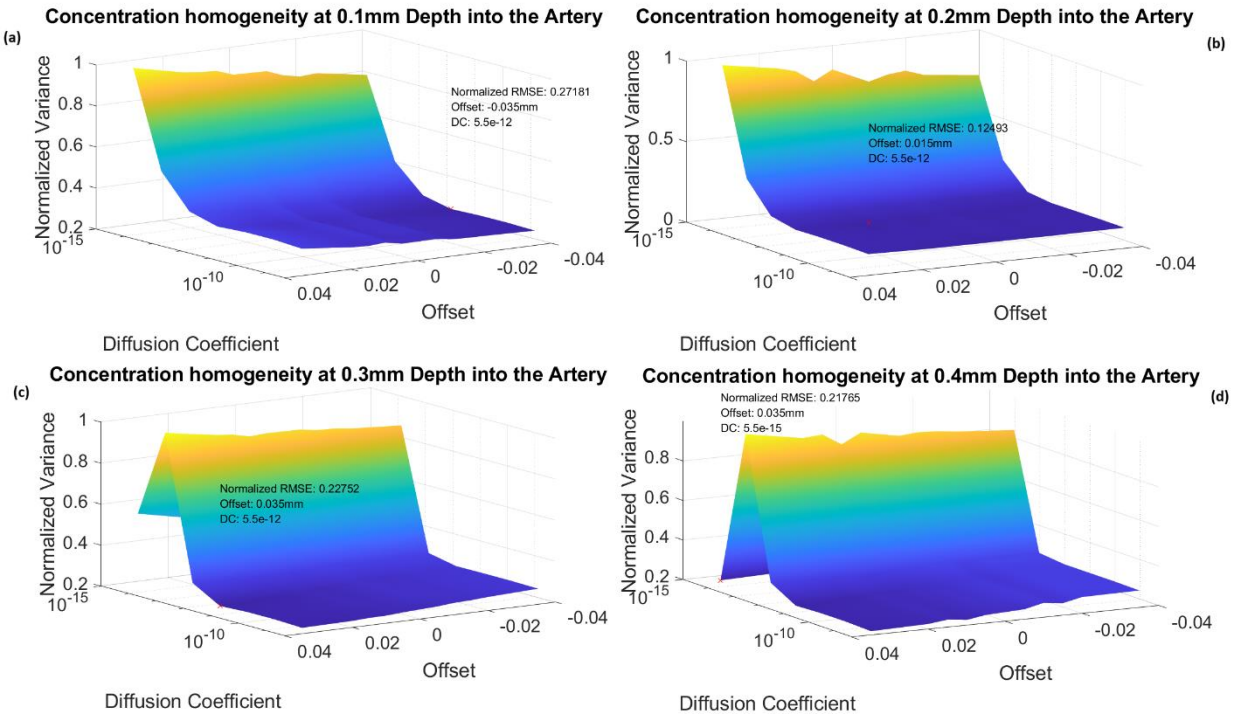

Figure 20: Variance plot for each design point at each depth into the artery after 3 days. Plot (a) is 0.1 mm, (b) is 0.2 mm, (c) is 0.3 mm, and (d) is 0.4 mm.

After 14 days, plotted in Figure 21, the points of minimal variance have changed from their locations after three days. The plots of particle variance along the 0.3 mm and 0.4 mm surfaces continue to show improved performance for scaffolds with larger cell offsets. For these two surfaces, the optimal design after 14 days is identical to the optimal design identified after three days. However, the geometric design points with the lowest variance for the 0.1 mm and 0.2 mm surfaces have moved. The optimal point for each of these surfaces is now at a location of a smaller surface area than the point identified after three days. The 0.2 mm surface joins the 0.3 mm and 0.4 mm surfaces at the lowest edge of the design space. The 0.1 mm surface moves from an offset of -0.035 mm to 0.02 mm between day three and day 14. The shape of the variance plot with respect to the diffusion coefficient remains the same. The overall trend

persists, but the location of the minimum value does change. Unlike the data from the 0.3 mm and 0.4 mm surfaces after three days, there is no peak and subsequent decrease in variance values after 14 days with a decreasing diffusion coefficient.

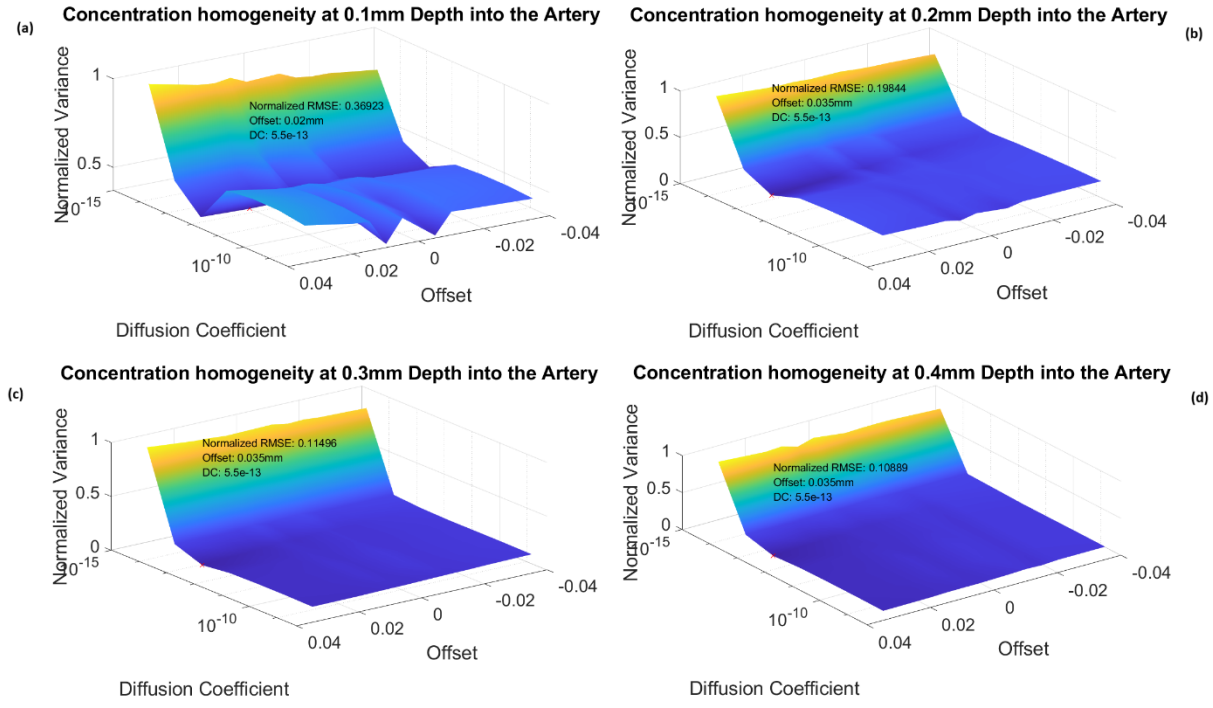

Figure 21: Variance plot for each design point at each depth into the artery after 14 days. Plot (a) is 0.1 mm, (b) is 0.2 mm, (c) is 0.3 mm, and (d) is 0.4 mm.

5.0 Discussion

The present study obtained results that have implications not only for the design of drug-eluting stents but also for future work in computationally aided stent design. The results presented above suggest that the scaffold geometry and particle diffusion coefficient have a

profound effect on the uniformity of particle distribution in the vascular wall. Previous work on this topic, conducted by Pant and others [63] [64], demonstrated similar results to those found in certain instances of this study. Pant's work focused on the distribution of particles in the artery volume. In this study, the distribution was analysed along two-dimensional surfaces at varying radial distances from the lumen. The findings here provide insight into the diffusion behaviour of the eluted particles and therapeutic insight into how different regions of the arterial tissue are affected by stent geometry. The main conclusions are presented in Table 5.

5.1 Steady state Simulation

The steady state simulations, characterized by constant blood velocity and particle flux, exhibited independence towards the particle diffusion coefficient. A steady state simulation assumes infinite time during its analysis. As a result, time-dependent factors will not influence the results. The diffusion coefficient, which is a measure of the diffusion rate of a particle, will have no impact on a steady state study. This result is observed in the simulations carried out in this study. The particle distribution and variance were both found to be independent of the diffusion coefficient.

While the diffusion coefficient failed to impact particle concentration homogeneity, the same cannot be said for the stent geometry parameter. At regions of the artery near the lumen, the flux of particles off the scaffold is the dominant factor influencing particle distribution. Accordingly, the pattern of the particles in the artery takes a shape that strongly resembles the scaffold geometry. The distribution experiences peaks in zones directly above struts and minimums in areas that are in the centre of open cells. There is little variance in particle density

within these areas, with a sudden transition in concentration occurring between the regions. In this study, the surface nearest to the lumen was at a radial distance of 0.1 mm. For this surface, the scaffold geometry that caused the lowest variance in particle distribution had the most negative cell offset. At this proximity to the lumen, the local peaks and minimums are unavoidable, due to the nature of particle diffusion. Displayed below in Figure 22 are contours of particle distribution on the 0.1 mm and 0.4 mm surfaces. The footprint of the scaffold geometry is visible on the 0.1 mm surface. For the stent with a 0 mm offset, as displayed below, the particle concentration in the regions directly above struts is larger than the regions above open cells by a factor of 10. With such a large disparity in particle density, the variance along this surface will be high. However, it can be minimized by increasing the area of high-density regions. The gap between particle count in open-cell and stent strut areas will always be large, but the overall variance can be reduced by changing the total size of each of these areas. In this case, the variance is minimized by producing the largest possible area of high particle count. This is done by increasing the size of the stent struts so that the stent's outer surface area is as large as possible.

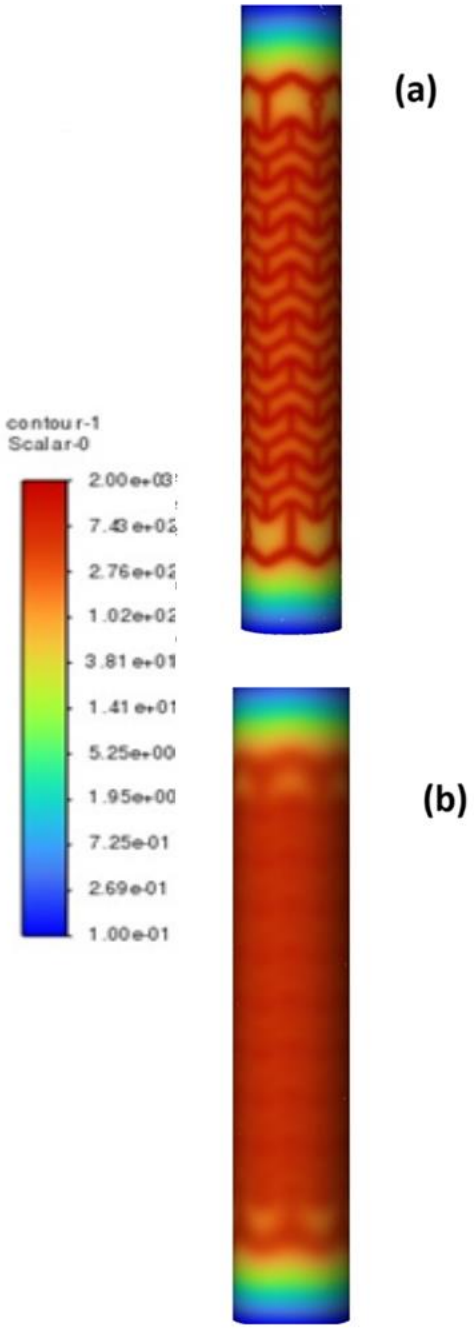

Figure 22: Contours of Steady state Particle Count.

Unlike the 0.1 mm surface, the imprint of the stent is not visible on the 0.4 mm surface. Rather than the flux of particles off the scaffold, the distribution is now more influenced by the natural

diffusion of the particles as they move through the artery. At this depth, the diffusion of the particles creates a far more even distribution. There are still regions where the particle density is high and regions where it is low, but the distinction is not as great and the transition between these regions is slow. This is also evident in Figures 13 through 16, where the peaks and valleys of particle count grow closer together as the distance from the lumen increases. This behaviour is similar for all cell offsets, but the magnitude of the particle density changes. The particle diffusion was defined by constant flux from the stent's outer surface, so the amount of particle diffusion is positively correlated with the surface area. The uniformity of particle distribution, which was determined by calculating the variance, is sensitive to the magnitude of particle concentration. As a result, the designs with the lowest magnitude particle count will have the most uniform distribution and lowest variance. A relationship that was also found by Pant et al. [63] [64]. Therefore, the scaffold design with the largest cell offset will provide the most uniform particle distribution. This analysis also holds for the 0.3 mm surface, which displayed an identical parameter location for the minimum variance to the 0.4 mm surface. Between the 0.1 mm and 0.3 mm surfaces, a transition occurs, where the uniformity is influenced by both the flux off the stent and the natural diffusion through the artery. This is displayed in the results for the 0.2 mm surface, where the ideal design point is an intermediate cell offset.

The blood-flow direction, which is visible in Figure 12, causes a higher particle concentration in the regions of the artery downflow from the stent. The particles that reach the lumen are swiftly carried downstream by the flow of blood. There, a small number may diffuse back into the artery. This distinction is only visible in Figure 12 and not Figure 22 due to the scales used in the respective figures. This indicates that though the flow direction does result in a higher

density of particles directly downstream of the stented region compared to the directly upstream region, the difference is negligible for any practical purposes and can likely be neglected.

5.2 Short Term Transient Simulation

Taking advantage of the short time scale, the six-second transient simulation was run using a physiologically accurate waveform as the inlet velocity. The effect of this waveform is complex fluid motion throughout the lumen, especially in the regions nearest to the stent scaffold. The results of this study indicate a trend that favors designs with more negative cell offsets. In the region of the design space with negative cell offsets, the influence of the diffusion coefficient is minimal. As the cell offset grows, the impact of the diffusion coefficient does too, with a general trend of larger coefficients providing results with lower variance. The cause of these trends is the low simulation time. Eluting stents are designed so that the particle diffusion takes place over a time scale that can be measured in days or even weeks. With a duration of only six seconds, this simulation ends with very few particles diffusing into the arterial tissue. As a result, the variance of the surfaces further from the artery is not as sensitive to the magnitude of particle diffusion as it is in the steady state study. Like the steady state study, there will be regions of relatively high and relatively low particle concentrations. The difference though, is that after six seconds, the particles will not have had time to diffuse into the open cell regions at any of the four surface depths. Instead, the particle distribution in all regions of the artery is mostly controlled by the flux of particles off the scaffold. This result can be seen in Figure 23 below, where the scaffold geometry is visible, even at the 0.4 mm surface.

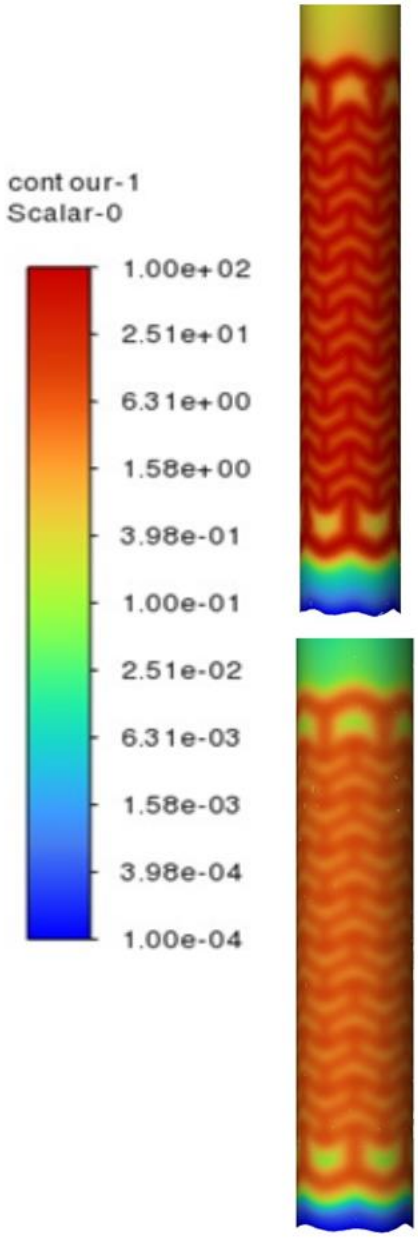

Figure 23: Contour of uds-0-scalar on the 0.1 mm (top) and 0.4 mm (bottom) surfaces after 6 seconds

In the regions of the design space where the diffusion coefficient does have a substantial impact on the variance, the improved performance by designs with larger diffusion coefficients is also a result of the time scale. The diffusion coefficient represents the speed at which particles move through the arterial tissue. In the cases where the coefficient is the smallest, the eluted particles

would not penetrate very far into the artery. Instead, the particles accumulate near the point where they first entered. On the other hand, a large diffusion coefficient causes particles to travel through the artery much quicker. After only six seconds, this is advantageous, as the particles will be able to diffuse through a larger portion of the artery, spreading out and creating a much more even distribution. This is why the designs with the largest diffusion coefficients were also found to have the lowest variance in particle distribution.

There appear to be two outliers that oppose the observed trends. The first is the location of minimum variance. Based on the normalized variance values, the design with the lowest variance had a cell offset of 0.01 mm and an arterial diffusion coefficient of $5.5 \cdot 10^{-12} \frac{m^2}{s}$. These two values each contradict the observed behaviour of more negative offsets and larger diffusion coefficients producing better uniformity. The second is the spike in variance that occurs at an offset of -0.015 mm. In either direction of this offset, there is no divergence from the behaviour predicted by the trend. At the time of writing, the causes for these two outliers remain unknown. They may be the result of errors in the simulation setup and calculation, but it is also equally possible that they demonstrate real and repeatable trends in the data. Future work is needed to analyse these anomalies and determine the origin of the observed behaviour.

5.3 Long Term Transient Simulation

The 14-day analysis allows for the consideration of particle diffusion and uniformity over an extended period. The unique quality of this simulation study is the presence of declining particle flux. A coated stent is implanted with a certain number of eluting particles in the coating. The concentration gradient between the stent coating and the arterial tissue causes

diffusion of the particles out of the stent and into the artery. As the particle count in the stent coating decreases and the count in the artery increases, the rate of diffusion will decline. The curve that was selected to model this decline was an exponential decay model with an initial value of 1.0 $(\frac{kg}{m^3} \cdot \frac{np}{m^2 s})$ at day zero, and a final value of 0.01 $(\frac{kg}{m^3} \cdot \frac{np}{m^2 s})$ at day 14. Implementation of a stent coated with the PMSC-NVs has yet to be done. The selected flux model is the result of discussions with Dotter Inc. (Seoul, Republic of Korea) and is based on the theoretical diffusion curve that will be attempted to be implemented. An analysis of the particle uniformity was carried out in two instances, after three days and after 14 days. Like the results from the six-second transient study, the 14-day simulation showed improved performance from designs with larger diffusion coefficients at both analysis time points. Though the timescale is much longer, the rationale for the behaviour is the same. A larger diffusion coefficient allows the particles to diffuse through the artery at a greater rate, resulting in a more even distribution.

Unlike the effect of the particle diffusion coefficient, the trends in the effect of stent geometry differed between day three and day 14. Within the first 72 hours, the particle diffusion is high relative to the subsequent 11 days. The result of this is conditions similar to the steady state study. This is also reflected in the results. After three days, the cell offsets that were identified as providing the highest level of uniformity were nearly identical to those found in the steady state simulations. As the simulated time passes, the particle flux continues to decline, following the depletion model. The particle distribution becomes less influenced by the flux off the stent and is more affected by the movement of the particles already within the arterial tissue. Many particles become lost, as they diffuse into the lumen, being carried away with the blood flow. After 14 days, the variance analysis reveals a shift in the optimal designs. The 0.2 mm surface

now joins the 0.3 mm and 0.4 mm surfaces, identifying the smallest stent surface as the design that provides the highest amount of particle concentration homogeneity. The 0.1 mm surface still identifies the largest optimal surface area of all the evaluation surfaces, but that optimal surface area is much smaller than the one found when analysing after three days. It has moved from the most negative offset of the design space, -0.035 mm, to 0.02 mm. A change in offset which results in a reduction of the stent surface area by 39%. The high flux at the start of the simulation sustains conditions and optimal results resembling the steady state condition for a period. During this time, the 0.1 mm surface displays a particle distribution pattern that takes the shape of the footprint of the outer surface of the stent. As time passes, the flux decline makes it so that this is no longer possible. Comparatively low numbers of particles are now diffusing into the artery. As a result, the high particle density in the regions above the struts starts to disperse, creating a more even distribution. The distinction between the above strut and above cell zones blur. Having a smaller area of high particle density and reducing the magnitude of particle concentration within those areas, results in better uniformity after 14 days. If the simulation were allowed to run further, it would be expected that the optimal design for the 0.1 mm surface would eventually join the others at the lower boundary of the cell offset design space.

Table 5: The main conclusions drawn from each simulation study.

Simulation Study	Main Conclusions
Steady state	At regions nearest to the artery, particle variance can be optimized using a stent design with a large outer surface area. Such as the case of the 0.1 mm surface. As the depth from the lumen grows, the optimal surface area declines. Based on the design space evaluated, once reaching a depth of 0.3 mm, the optimal variance will be achieved by a design with the smallest allowable outer surface area.
Short Term Transient	A larger diffusion coefficient will generally result in improved particle variance. The optimal stent geometry will be one with a large outer surface area. Unlike the steady state case, these findings do not vary as the depth from the lumen grows.
Long Term Transient	A decrease in diffusion coefficient results in an exponential increase in particle variance. This was found after 3 days and after 14 days. In the first 3 days, the stent geometry displays trends in particle variance nearly identical to the steady state case, concerning the depth into the artery. After 14 days, there is a significant shift towards smaller outer surface areas producing the most even particle distribution.

5.4 Comparing Simulation Studies

The simulation studies analysed in this thesis cover a broad range of simulation conditions. The influence of short, long, and infinite timescales was examined. So were steady and transient flows and particle fluxes. The magnitude of the effect of the diffusion coefficient varied between the three cases and is due to the variation in simulation length. In the six-second simulation, the designs with larger diffusion coefficients experienced variance values that were less than 1% of the maximum variance. For the 14-day simulations, the variance values of the large diffusion coefficient designs were 10-40% of the maximum variance. As the timescale increases, the influence of rate-dependent variables declines. After six seconds, the influence of the diffusion coefficient is enormous. After 14 days the impact is reduced but still evident. After an infinite period, which is modeled by the steady state simulation, the influence is erased.

The volatility displayed by the six-second transient simulation results is unique among the studies analysed. The 14-day and steady state simulations resulted in variance surfaces that are much smoother. What separates the six-second simulation study from the other two is the extremely short timescale and transient inlet velocity. The physiological velocity waveform causes complex and changing patterns of wall stresses. Though the flow-mediated uptake is negligible, a result found in both this study and previous work [58], these wall stresses influence the particle variance in the artery and could be partially to blame for the volatility of the six-second simulation results. The short timescale is also likely at fault. At such a short duration, the particles will not have had time to diffuse into many regions of the artery, leading to large variations in distribution. As a result, the variance values for each design point will be very

sensitive to changes in either diffusion coefficient or cell offset. The simulations with longer durations have a much lower sensitivity to changes in parameters, due to the longer timescale, and subsequently do not experience as much volatility in their results.

5.5 Limitations and Future Work

This thesis endeavors to contribute insights into the field of drug-eluting stent technology. However, it is essential to acknowledge the inherent limitations of the simulations that shape the scope and application of the findings. There are restrictions in simulation accuracy that are universal to all three simulation cases, but also those that are unique to each. The shared limitations relate to the arterial construction, the number of design points, and the position of the stent relative to the artery wall. The artery was modeled as isotropic and uniform, which is far from reality. As discussed in the introduction, the artery is composed of several layers, each with unique materials and properties. Additionally, stenting is most commonly used to treat atherosclerosis. Rather than simulating the arterial layers and the presence of atherosclerotic plaque, the artery was modeled as homogeneous. The diffusion performance of the eluted particles would be expected to vary throughout different regions of the artery. Instead, the artery was modeled as a uniform material, and thus, the diffusional behaviour of the particles is constant throughout. The values found in this study likely overpredict the particle uniformity, as the presence of atherosclerotic plaque and arterial tissue are composed of varying materials would cause an increase in particle distribution variance. Another limitation in artery construction is its shape. In the case of this experiment, the artery is simulated as straight. However, stents are often implanted in curved or branched arterial sections. The flow and corresponding wall stresses would be different than those modeled in

this study as a result. The findings are therefore only applicable to instances of straight arterial sections, as the addition of curvature has been found to greatly impact the drug diffusion profile within the artery of drug-eluting stent simulations [72]. An additional limitation is the number of design points. In total, 77 cases were evaluated. The design points were comprised of a combination of 11 cell offsets and seven diffusion coefficients. As a result, the variance distribution throughout the design space is coarse. The results display optimal values within the defined design space coarseness. In future work, a less coarse design space should be analyzed to determine local trends and global optimal points. The final shared limitation is the apposition of the stent to the artery wall. It has been found that the distribution of particles in the artery becomes significantly impacted by flow pulsatility when the struts are not fully apposed to the arterial wall [58] [73]. When a gap is present, rather than the particles diffusing directly into the artery, they enter the blood first. In an ideal implantation, the struts will always contact the arterial surface, but imperfect stent expansion causes this to not always occur. In the present study, this factor was neglected.

The major limitation of the steady state simulation is that it models impossible conditions. It assumes constant blood flow, an unending supply of eluting particles, and infinite time. These components contradict each other. Over an extended period, as the 14-day case models, the store of particles on the stent declines, resulting in a reduction in the flux of particles into the artery. The steady state simulation ignores this. As well, the blood flow does not accurately represent physiological flow conditions. Pulsatility is overlooked, and the flow is steady. A limitation that is also present for the 14-day simulation.

Apart from the flow behaviour, the 14-day simulation is also influenced by the flux model. The flux-time curve used to control the particle diffusion is relatively arbitrary. There is currently no experimental data available that can be used to confidently determine the PMSC-NVs diffusion behaviour. As a result, an assumption must be made regarding the decline in particle flux. To assess the impact of this assumption, a secondary analysis was run where the exponential decay of the particle flux is reduced by half. This resulted in a particle flux by the 14^{th} day that is ten times greater than the original model used. After three days the results between the two flux models were the same, but, after 14 days they varied. The slower decay model found that after 14 days, the optimal design points were identical to those found after three days. So, the slower the decay model, the longer the period where the results match the steady state case. These findings do not invalidate the results found from the original flux model, but it does mean that the findings are sensitive to the model selected, and thus are only applicable to that specific model at those specific time points.

Future work is required to both validate and improve upon the results found in this study. At present, the data obtained from the simulation is unvalidated by experimental work. This needs to be done to confirm the accuracy and reliability of the findings. Another consideration for future work is to conduct an optimization analysis. In this study, the design space was explored, but not optimized. The results display general trends, but optimal values are not discreetly identified. Additionally, the responsibilities of an eluting stent are not the eluted particle uniformity alone. Instead, the stent must also resist several forms of mechanical loading, such as forces during expansion and compression forces following implantation. Further work should

be done, linking the particle eluting performance with the structural performance. In this way, the designed stent can be optimized for its two key obligations.

6.0 Conclusion

Percutaneous coronary interventions have revolutionized the treatment of atherosclerosis. Though the rate of patient mortality has plummeted since the advent of coronary stents, complications still occur. By conducting an analysis of particle distribution following eluting stent implantation, this study aimed to determine the influence that the scaffold geometry and particle diffusion properties have on eluting stent performance. The trend of the diffusion coefficient data demonstrated that a larger coefficient produces the most uniform particle distribution. This trend was observed for all the cases examined. The scaffold geometry, on the other hand, demonstrated trends that changed spatially and temporally. When the eluted medication is required to target shallow sections of the arterial wall, a design with a large surface area is ideal. As the depth is increased, a design with a smaller outer surface, and thus, a lower particle diffusion, will optimize particle uniformity. Over time, the inevitable decline in particle flux leads to optimal uniformity occurring via designs with reduced outer surfaces, when compared to their younger counterparts.

The findings presented above also demonstrate the validity of using steady state simulation cases for in-silico eluting stent design analysis. The steady state simulation results predicted the same pattern in optimal stent geometry as the transient simulation for up to three days with the original flux decay model, and up to 14 days for the half-decay model. Though the steady state

cases underpredict the variance difference between design points, the correct trend relating the particle uniformity and the stent geometry is still identified.

Stenting is not a “one size fits all” treatment method. The scaffold geometry needs to be adjusted based on the size of the artery, the selected medication, and the targeted duration of action of said medication. The largest artery in the body is the aorta. With a wall thickness of such a magnitude, optimal performance would occur with a small stent outer surface area. However, cardiovascular stents are also used in arteries with diameters as small as 1.5 mm [74]. When applied in these circumstances, the data from this study suggest that a scaffold design with a large outer surface is best suited for such a thin arterial wall. The design can be improved further by considering the diffusion-time curve. Though the implantation may occur within a thin artery, the larger eluting surface is not beneficial if the duration of therapeutic action lasts long enough that the particle diffusion off the stent becomes negligible.

References

[1] M. Cesare, H. Bixby, T. Gaziano, L. Hadeed, C. Kabudula, D. McGhie, J. Mwangi, B. Pervan, P. Perel, D. Pineiro, S. Taylor and F. Pinto, "World Heart Report 2023," World Heart Foundation, Geneva, 2023.

[2] P. A. S. Ponikowske, K. Alhabib, M. Cowie, T. Force, S. Hu, T. Jaarsma, H. Krum, V. Rastogi, L. Rohde, U. Samal, H. Shimokawa, B. Siswanto, K. Sliwa and G. Filippatos, "Heart failure: preventing disease and death worldwide," *ECS Heart Failure,* vol. 1, no. 1, pp. 4-25, 2014.

[3] N. Jones, A. Roalfe, I. Adoki, R. Hobbs and C. Taylor, "Survival of Patients with Chronic Heart Failure in the Community: a Systematic Review and Meta-Analysis," *European Journal of Heart Failure,* vol. 21, no. 11, pp. 1306-1325, 2019.

[4] S. Dhruva, C. Parzynski, G. Gamble, J. Curtis, N. Desai, R. Yeh, F. Masoudi, R. Kuntz, R. Shaw, D. Marinac-Dabic, A. Sedrakyan, S.-L. Normand, H. Krumholz and J. Ross, "Attribution of Adverse Events Following Coronary Stent Placement Identified Using Administrative Claims Data," *Journal of American Heart Association,* vol. 9, no. 4, 2020.

[5] S. Shrestha, J. Patel, G. Hollander and J. Shani, "Coronary Artery Stents," *Consultant 360,* vol. 60, no. 6, 2020.

[6] D. Holmes, D. Kereiakes, S. Garg, P. Serruys, G. Dehmer, S. Ellis, D. Williams, T. Kimura and D. Moliterno, "Stent Thrombosis," *Journal of the American College of Cardiology,* vol. 56, no. 17, pp. 1357-1365, 2010.

[7] "What Are Stents?," National Heart, Lung, and Blood Institute, 24 March 2022. [Online]. Available: https://www.nhlbi.nih.gov/health/stents. [Accessed 6 September 2023].

[8] J.-K. Yoon, D.-H. Kim, M.-L. Kang, H.-K. Jang, H.-J. Park, J. B. Lee, S. W. Yi, H.-S. Kim, S. Baek, D. B. Park, J. You, S.-D. Lee, Y. Sei, S. I. Ahn, Y. M. Shin, C. S. Kim and S. Bae, "Anti-Atherogenic Effect of Stem Cell Nanovesicles Targeting Disturbed Flow Sites," *Small,* vol. 16, no. 16, 2020.

[9] A. Mercadante and A. Raja, "Anatomy, Arteries," National Library of Medicine, 6 March 2023. [Online]. Available: https://www.ncbi.nlm.nih.gov/books/NBK547743/. [Accessed 11 September 2023].

[10] R. Lloyd, "Synthetic Blood Vessels Not Such a Stretch," Live Science, 18 June 2006. [Online]. Available: https://www.livescience.com/815-synthetic-blood-vessels-stretch.html. [Accessed 28 September 2023].

[11] C. Ethier and C. Simmons, Introductory Biomechanics From Cells to Organisms, Cambridge: Cambridge University Press, 2007.

[12] P. Libby, "Atherosclerosis: The New View," *Scientific American,* vol. 286, no. 5, pp. 46-55, 2002.

[13] P. Libby, "The changing landscape of atherosclerosis," *Nature,* vol. 592, pp. 524-533, 2021.

[14] B. Wadstrom, K. Pedersen, A. Wulff and B. Nordestgaard, "Inflammation compared to low-density lipoprotein cholesterol: two different causes of atherosclerotic cardiovascular disease," *Current Opinion on Lipidology,* vol. 34, no. 3, pp. 96-104, 2023.

[15] G. Ciccarelli, S. Conte, G. Cimmino, P. Maiorano, A. Morrione and A. Giordano, "Mitochondrial Dysfunction: The Hidden Player in the Pathogenesis of Atherosclerosis?," *International Journal of Molecular Sciences,* vol. 24, no. 2, 2023.

[16] P. Theofilis, E. Oikonomou, K. Tsiofis and D. Tousoulis, "The Role of Macrophages in Atherosclerosis: Pathophysiologic Mechanisms and Treatment Considerations," *International Journal of Molecular Sciences,* vol. 24, no. 11, 2023.

[17] C. Dotter and M. Judkins, "Transluminal Treatment of Arteriosclerotic Obstruction," *Circulation,* vol. 30, no. 5, pp. 654-670, 1964.

[18] D. Losordo, K. Rosenfield, A. Pieczek, K. Baker, M. Harding and J. Isner, "How does angioplasty work? Serial analysis of human iliac arteries using intravascular ultrasound.," *Circulation,* vol. 86, no. 6, pp. 1845-1858, 1992.

[19] D. Faxon, T. Sanborn and C. Hauenschild, "Mechanism of angioplasty and its relation to restenosis," *The American Journal of Cardiology,* vol. 60, no. 3, pp. 5-9, 1987.

[20] J. Bittl, "Advances in Coronary Angioplasty," *New England Journal of Medicine,* vol. 335, no. 17, pp. 1290-1302, 1996.

[21] A. Nichols, R. Smith, A. Berke, R. Shlofmitz and E. Powers, "Importance of balloon size in coronary angioplasty," *Journal of the American College of Cardiology,* vol. 13, no. 5, pp. 1094-1100, 1989.

[22] P. Steele, J. Chsebro, A. Stanson, D. Holmes, M. Dewanjee, L. Badimon and V. Fuster, "Balloon angioplasty. Natural history of the pathophysiological response to injury in a pig model.," *Circulation Research,* vol. 57, no. 1, pp. 105-112, 1985.

[23] C. Grines, D. Cox, G. Stone and E. Garcia, "Coronary Angioplasty with or without Stent Implantation for Acute Myocardial Infarction," *New England Journal of Medicine,* vol. 341, no. 26, pp. 1949-1956, 1999.

[24] J. Palmaz, "Balloon-Expandable Intravascular Stent," *American Journal of Radiology,* vol. 150, no. 6, pp. 1263-1269, 1988.

[25] U. Sigwart, J. Puel, V. Mirkovitch, F. Joffre and L. Kappenberger, "Intravascular Stents to Prevent Occlusion and Re-Stenosis after Transluminal Angioplasty," *The New England Journal of Medicine,* vol. 316, pp. 701-706, 1987.

[26] P. Serruys, P. Jaegere, F. Kiemeneij and C. Macaya, "A Comparison of Balloon-Expandable-Stent Implantation with Balloon Angioplasty in Patients with Coronary Artery Disease," *The New England Journal of Medicine,* vol. 331, pp. 489-495, 1994.

[27] M. Levine, B. Leonard, J. Burke, I. Nash, R. Safian, D. Diver and D. Baim, "Clinical and angiographic results of balloon-expandable intracoronary stents in right coronary artery stenoses," *Journal of the American College of Cardiology,* vol. 16, no. 2, pp. 332-339, 1990.

[28] A. Betriu, M. Masotti, A. Serra, J. Alonso, F. Fernandez-Aviles, F. Gimeno, T. Colman, J. Zueco, J. Delcan, E. Garcia and J. Calbuig, "Randomized Comparison of Coronary Stent Implantation and Balloon Angioplasty in the Treatment of De Novo Coronary Artery Lesions (START): a Four-Year Follow-Up," *Journal of the American College of Cardiology,* vol. 34, no. 5, pp. 1498-1506, 1999.

[29] T. Kimura, H. Yokoi, Y. Nakagawa and T. Tamura, "Three-Year Follow-up after Implantation of Metallic Coronary-Artery Stents," *The New England Journal of Medicine,* vol. 334, pp. 561-567, 1996.

[30] J. Iqbal, J. Gunn and P. Serruys, "Coronary stents: historical development, current status and future directions," *British Medical Bulletin,* vol. 106, no. 1, pp. 193-211, 2013.

[31] L. Grenacher, S. Rohde, E. Ganger, J. Deutsch, G. Kauffmann and G. Richter, "In Vitro Comparison of Self-Expanding Versus Balloon-Expandable Stents in a Human Ex Vivo Model," *CardioVascular and Interventional Radiology,* vol. 29, pp. 249-254, 2006.

[32] H. Krankenberg, T. Zeller, M. Ingwersen, J. Schmalstieg, H. Gissler, S. Nikol, I. Baumgartner and N. Diehm, "Self-Expanding Versus Balloon-Expandable Stents for Iliac Artery Occlusive Disease: The Randomized ICE Trial," *J Am Coll Cardiol Intv.,* vol. 10, no. 16, pp. 1694-1704, 2017.

[33] R. Han, R. Schwartz, Y. Kobayashi, S. Wilson, J. T. Mann, M. Sketch, R. Safian, A. Lansky, J. Popma, P. Fitzgerald, I. Palacios, M. Chazin-Caldie and S. Goldberg, "Comparison of self-expanding and balloon-expandable stents for the reduction of restenosis," *The American Journal of Cardiology,* vol. 88, no. 3, pp. 253-259, 2001.

[34] T. Schmidt and J. D. Abbot, "Coronary Stents: History, Design, and Construction," *Journal of Clinical Medicine,* vol. 7, no. 6, 2018.

[35] P. Moreno, I. Palacios, M. Leon, J. Rhodes, V. Fuster and J. Fallon, "Histopathologic comparison of human coronary in-stent and post-balloon angioplasty restenotic tissue," *The American Journal of Cardiology,* vol. 84, no. 4, pp. 462-466, 1999.

[36] C. Chaabane, F. Otsuka, R. Virmani and M.-L. Bochaton-Piallat, "Biological responses in stented arteries," *Cardiovascular Research,* vol. 99, no. 2, pp. 353-363, 2013.

[37] A. Finn, G. Nakazawa, M. Joner, F. Kolodgie, E. Mont and H. V. R. Gold, "Vascular Responses to Drug Eluting Stents," *Arteriosclerosis, Thrombosis, and Vascular Biology,* vol. 27, no. 7, pp. 1500-1510, 2007.

[38] A. Lansky, C. Hyung, C. Pietras and Y. Hussain, "Refining drug-eluting stent technologies: from engineering to basic science," *European Heart Journal,* vol. 42, no. 18, pp. 1770-1772, 2021.

[39] S. Bangalore, B. Toklu, N. Amoroso, M. Fusaro, S. Kumar, E. Hannan, D. Faxon and F. Feit, "Bare metal stents, durable polymer drug eluting stents, and biodegradable polymer drug eluting stents for coronary artery disease: mixed treatment comparison meta-analysis," *The BMJ,* 2013.

[40] B. Lagerqvist, S. James, U. Stenestrand, J. Lindback, T. Nilsson and L. Wallentin, "Long-Term Outcomes with Drug-Eluting," *The New England Journal of Medicine,* vol. 356, no. 10, pp. 1009-1019, 2007.

[41] S. Bangalore, S. Kumar, M. Fusaro, N. Amoroso, M. Attubato, F. Feit, D. Bhatt and J. Slater, "Short- and Long-Term Outcomes With Drug-Eluting and Bare-Metal Coronary Stents," *Circulation,* vol. 125, no. 23, pp. 2873-2891, 2012.

[42] T. Palmerini, G. Biondi-Zoccai, D. Riva, A. Mariani, P. Genereux, A. Branzi and G. Stone, "Stent Thrombosis With Drug-Eluting Stents: Is the Paradigm Shifting?," *Journal of the American College of Cardiology,* vol. 62, no. 21, pp. 1915-1921, 2013.

[43] E. Secemsky, H. Kundi, I. Weinberg, M. Schermerhorn, J. Beckman, S. Parikh, M. Jaff, J. Mustapha, K. Rosenfield and R. Yeh, "Drug-Eluting Stent Implantation and Long-Term Survival Following Peripheral Artery Revascularization," *Journal of the American College of Cardiology,* vol. 73, no. 20, pp. 2636-2638, 2019.

[44] L. Mauri, T. Silbaugh, R. Wolf, K. Zelevinsky, A. Lovett, Z. Zhou, F. Resnic and S.-L. Normand, "Long-Term Clinical Outcomes After Drug-Eluting and Bare-Metal Stenting in Massachusetts," *Circulation,* vol. 118, no. 18, pp. 1817-1827, 2008.

[45] K. Katsanos, S. Spiliopoulos, P. Kitrou, M. Krokidis and D. Karnabatidis, "Risk of Death Following Application of Paclitaxel-Coated Balloons and Stents in the Femoropopliteal Artery of the Leg: A Systematic Review and Meta-Analysis of Randomized Controlled Trials," *Journal of the American Heart Association,* vol. 7, no. 24, 2018.

[46] H. Y. Kim, S. Kwon, W. Um, S. Shin, C. H. Kim, J. H. Park and B.-S. Kim, "Functional Extracellular Vesicles for Regenerative Medicine," *Small,* vol. 65, no. 69, 2022.

[47] W. Wang, Y. Zhao, H. Li, Y. Zhang, X. Jia, C. Wang, P. Zhu, J. Wang and Y. Hou, "Exosomes secreted from mesenchymal stem cells mediate the regeneration of endothelial cells treated with rapamycin by delivering pro-angiogenic microRNAs," *Experimental Cell Research,* vol. 399, no. 1, pp. 1124-1149, 2021.

[48] S. Hu, Z. Li, D. Shen, D. Zhu, K. Huang, T. Su, P.-U. Dinh, J. Cores and K. Cheng, "Exosome-eluting stents for vascular healing after ischaemic injury," *Nature Biomedical Engineering,* vol. 5, pp. 1174-1188, 2021.

[49] M. Grundeken and M. Beijk, "A Narrative Review of Ultrathin-strut Drug-eluting Stents: The Thinner the Better?," *Heart International,* vol. 15, no. 2, pp. 84-93, 2021.

[50] F. Yan, W.-t. Jiang, T.-h. Zheng, Y.-b. Fan and Z. Liu, "Numerical analysis of effects from drug-eluting stent height on drug concentration and all shear stress distribution," *Journal of Medical Biomechanics,* pp. 451-455, 2012.

[51] S. Bangalore, B. Toklu, N. Patel, F. Feit and G. Stone, "Newer-Generation Ultrathin Strut Drug-Eluting Stents Versus Older Second-Generation Thicker Strut Drug-Eluting Stents for Coronary Artery Disease," *Circulation,* vol. 138, no. 20, pp. 2216-2226, 2018.

[52] K. Kolandaivelu, R. Swaminathan, W. Gibson, V. Kolachalama, K.-L. Nguyen-Ehrenreich, V. Giddings, L. Coleman, G. Wong and E. Edelman, "Stent Thrombogenicity Early in High-Risk Interventional Settings Is Driven by Stent Design and Deployment and Protected by Polymer-Drug Coatings," *Circulation,* vol. 123, no. 13, pp. 1400-1409, 2011.

[53] Y. Chen, Y. Xiong, W. Jiang, J. Chen, M. Guo, Q. Wang and Y. Fan, "NUMERICAL STUDY ON THE EFFECTS OF THE NUMBER AND GEOMETRIES OF DRUG-ELUTING STENT LINKS ON THE DRUG CONCENTRATION," *Journal of Mechanics in Medicine and Biology,* vol. 14, no. 5, 2014.

[54] J. Suh, D.-W. Park, J.-Y. Lee, I. H. Jung, S.-W. Lee, Y.-H. Kim, C. W. Lee, S.-S. Cheong, J.-J. Kim, S.-W. Park and S.-J. Park, "The Relationship and Threshold of Stent Length With Regard to Risk of Stent Thrombosis After Drug-Eluting Stent Implantation," *Journal of the American College of Cardiology: Cardiovascular Interventions,* vol. 3, no. 4, pp. 383-389, 2010.

[55] T. Gundert, A. Marsden, W. Yang and J. Ladisa, "Optimization of Cardiovascular Stent Design Using Computational Fluid Dynamics," *Journal of Biomechanical Engineering,* vol. 134, no. 1, 2012.

[56] Y. Li, Y. Wang, Z. Shen, F. Miao, J. Wang, Y. Sun, S. Zhu, Y. Zheng and S. Guan, "A biodegradable magnesium alloy vascular stent structure: Design, optimisation and evaluation," *Acta Biomaterialia,* vol. 142, pp. 402-412, 2022.

[57] G. Karanasiou, M. Papafaklis, C. Conway, L. Michalis, R. Tzafriri, E. Edelman and D. Fotiadis, "Stents: Biomechanics, Biomaterials, and Insights from Computational Modeling," *Annals of Biomedical Engineering,* vol. 45, pp. 853-872, 2017.

[58] P. Vijayaratnam, J. Reizes and T. Barber, "Flow-Mediated Drug Transport from Drug-Eluting Stents is Negligible: Numerical and In-vitro Investigations," *Annals of Biomedical Engineering,* vol. 47, pp. 878-890, 2019.

[59] J. Song, S. Kouidri and F. Bakir, "Review on the numerical investigations of mass transfer from drug eluting stent," *Biocybernetics and Biomedical Engineering,* vol. 41, no. 3, pp. 1057-1070, 2021.

[60] V. Kolachalama, A. Tzafriri, D. Arifin and E. Edelman, "Luminal flow patterns dictate arterial drug deposition in stent-based delivery," *Journal of Controlled Release,* vol. 133, no. 1, pp. 24-30, 2009.

[61] J. Ako, H. Bonneau, Y. Honda and P. Fitzgerald, "Design criteria for the ideal drug-eluting stent," *American Journal of Cardiology,* vol. 100, no. 8, pp. S3-S9, 2007.

[62] N. Bulman-Fleming, R. Mongrain and O. Bertrand, "Numerical Simulations for The Evaluation of Material Diffusion Characteristics in Eluting Coronary Stents," *Computational Molecular Biophysics and Bioinformatics Study Environment Proceedings,* vol. 27, 2002.

[63] S. Pant, N. Bressloff and G. Limbert, "Geometry parameterization and multidisciplinary constrained optimization of coronary stents," *Biomechanics and Modeling in Mechanobiology,* vol. 11, pp. 61-82, 2012.

[64] S. Pant, G. Limbert, N. Curzen and N. Bressloff, "Multiobjective design optimisation of coronary stents," *Biomaterials,* vol. 32, no. 31, pp. 7755-7773, 2011.

[65] H. Walker, W. Hall and J. Hurst, Clinical Methods: The History, Physical, and Laboratory Examinations. 3rd edition., Boston: Butterworths, 1990.

[66] J. Berry, A. Santamarina, J. Moore, S. Roychowdhury and W. Routh, "Experimental and computational flow evaluation of coronary stents," *Annals of Biomedical Engineering,* vol. 28, no. 4, pp. 386-398, 2000.

[67] O. Kwon, M. Krishnamoorthy, Y. Cho, J. Sankovic and R. Banerjee, "Effect of Blood Viscosity on Oxygen Transport in Residual Stenosed Artery Following Angioplasty," *Journal of Biomechanical Engineering,* vol. 130, 2008.

[68] E. Nagel, T. Thouet, C. Klein, S. Schalla, A. Bornstedt, B. Schnakenburg, J. Hug, E. Wellnhofer and E. Fleck, "Noninvasive Determination of Coronary Blood Flow Velocity With Cardiovascular Magnetic Resonance in Patients After Stent Deployment," *Circulation,* vol. 107, no. 13, pp. 1738-1743, 2003.

[69] C. Feldman, O. Ilegbusi, Z. Hu, R. Nesto, S. Waxman and P. Stone, "Determination of in vivo velocity and endothelial shear stress patterns with phasic flow in human coronary arteries: A methodology to predict progression of coronary atherosclerosis," *American Heart Journal,* vol. 143, no. 6, pp. 931-939, 2002.

[70] N. Kastelowitz and H. Yin, "Exosomes and Microvesicles: Identification and Targeting By Particle Size and Lipid Chemical Probes," *Chembiochem,* vol. 15, no. 7, pp. 923-928, 2014.

[71] R. Pizzolato and J. Romero, "Neurosonology and noninvasive imaging of the carotid arteries," *Handbook of Clinical Neurology,* vol. 135, no. 3, pp. 165-191, 2016.

[72] J. Escuer, I. Aznar, C. McCormick, E. Pena, S. McGinty and M. Martinez, "Influence of vessel curvature and plaque composition on drug transport in the arterial wall following drug-eluting stent implantation," *Biomechanics and Modeling in Mechanobiology,* vol. 20, pp. 767-786, 2021.

[73] C. O'Brien, V. Kolachlama, T. Barber, A. Simmons and E. Edelman, "Impact of flow pulsatility on arterial drug distribution in stent-based therapy," *Journal of Controlled Release,* vol. 168, no. 2, pp. 115-124, 2013.

[74] M. Wybraniec, P. Banka, T. Bochenek, T. Roleder and K. Mizia-Stec, "Small vessel coronary artery disease: How small can we go with myocardial revascularization?," *Cardiology Journal,* vol. 28, no. 5, pp. 767-778, 2020.